JGR Earth Surface

RESEARCH ARTICLE
10.1029/2021JF006480

Uranium Isotopic Composition and Constraints on the Provenance of the Qinghai-Tibet Plateau's Surface Dust

Xiaoyu Jiao[1,2], Zhiwen Dong[1,3], Eric J. R. Parteli[4], Janice Brahney[5], Ting Wei[1,2], Marcelli Augusto[6,7], Junsheng Nie[8], Jiawen Ren[1,2], and Xiang Qin[1,9]

[1]State Key Laboratory of Cryosphere Sciences, Northwest Institute of Eco-Environment and Resources, Chinese Academy of Sciences, Lanzhou, China, [2]University of Chinese Academy of Sciences, Beijing, China, [3]CAS Center for Excellence in Tibetan Plateau Earth Sciences, Chinese Academy of Sciences (CAS), Beijing, China, [4]Department of Physics, University of Duisburg-Essen, Duisburg, Germany, [5]Department of Watershed Sciences, Utah State University, Logan, UT, USA, [6]INFN–LNF, Frascati, Italy, [7]CNR - Istituto Struttura Della Materia and Elettra-Sincrotrone Trieste, Basovizza Area Science Park, Trieste, Italy, [8]Key Laboratory of Western China's Environmental Systems (Ministry of Education), Lanzhou University, Lanzhou, China, [9]Qilian Mountain Glacier and Ecological Environment Research Station, Chinese Academy of Sciences, Lanzhou, China

Key Points:

- We investigated the $^{234}U/^{238}U$ isotope ratios of surface dust samples collected at various locations on the Tibetan Plateau
- The ($^{234}U/^{238}U$) isotopes reflected the influence of regional tectonic evolution, landscape dynamics, and glacier erosion processes
- Uranium isotopes in Tibetan Plateau dust are regionally distinguishable and thus represent a powerful tracer for dust source identification

Supporting Information:

Supporting Information may be found in the online version of this article.

Correspondence to:

Z. Dong,
dongzhiwen@lzb.ac.cn

Citation:

Jiao, X., Dong, Z., Parteli, E. J. R., Brahney, J., Wei, T., Augusto, M., et al. (2022). Uranium isotopic composition and constraints on the provenance of the Qinghai-Tibet Plateau's surface dust. *Journal of Geophysical Research: Earth Surface*, *127*, e2021JF006480. https://doi.org/10.1029/2021JF006480

Received 13 OCT 2021
Accepted 23 FEB 2022

Author Contributions:

Conceptualization: Zhiwen Dong, Jiawen Ren
Investigation: Xiaoyu Jiao, Zhiwen Dong, Janice Brahney, Ting Wei, Xiang Qin
Methodology: Eric J. R. Parteli, Xiang Qin
Resources: Zhiwen Dong, Jiawen Ren
Validation: Marcelli Augusto
Visualization: Ting Wei, Junsheng Nie, Xiang Qin
Writing – original draft: Xiaoyu Jiao, Zhiwen Dong
Writing – review & editing: Eric J. R. Parteli, Janice Brahney, Ting Wei, Marcelli Augusto, Junsheng Nie, Jiawen Ren

Abstract The production and emission of aeolian dust can provide key information on the contemporary and historical links between geological evolution and climate. Here we use $^{234}U/^{238}U$ isotope ratios and the uranium (U) comminution age method on samples collected from Qinghai-Tibet Plateau (TP) surface dust and glacier snowpack/cryoconites to determine the erosion and potential transport provenance of the dust, regardless of petrological origin. The spatial variation of the ($^{234}U/^{238}U$) isotope ratios of TP dust showed relatively high values in the Songpan-Ganzi-Hoh Xil, Himalayan and the Kunlun-Qaidam-Qilian terranes, while showing relatively low ($^{234}U/^{238}U$) values in Lhasa and Qiangtang terranes, but among all samples the highest value appeared in the glaciation zone. Dust collected from nearby glacial areas with rugged terrain (e.g., the Qilian and Himalayan Mountains) have higher ($^{234}U/^{238}U$) values than those collected in the topologically flat non-glacial areas. These differences are consistent with elevated erosion rates and dust comminution-transport processes in glacial areas, which yield a major source for large quantities of fresh comminuted particles. Compared to sediments from other regions of the globe, the ($^{234}U/^{238}U$) values of the typical aeolian sinks (such as loess on the Loess Plateau and ice core dust, etc.) are generally lower in comparison to areas with high elevations where erosion rates are high. The ($^{234}U/^{238}U$) isotope values of TP dust tend to fall between the high-elevation sites and the dust sinks, indicating the combined influence of short comminution times (tectonics, landscape dynamics, and glacial erosion) and long residence time on the TP. When compared with other central Asian dust sources, U-Nd-Sr isotope signatures in TP dust are distinct and can be thus used as an effective tracer of dust provenance. Using U isotopes, we show that dust originating from the TP undergoes long-range transport and constitutes potentially significant component of the Asian and Northern Hemisphere atmospheric dust load.

Plain Language Summary This work is the first to measure the ^{234}U and ^{238}U isotopic composition of surface dust particles in the cryospheric regions of the Tibetan Plateau and to use the uranium (U) comminution age method to reveal the spatial distribution and variation of the ($^{234}U/^{238}U$) values and the evolution processes of Tibetan Plateau dust. In addition, we use the U isotopic composition of dust from several snowpack and cryoconite samples from glaciers in the Tibetan Plateau to constrain Tibetan Plateau dust transport distances and major sink areas. Together, the research provides new insights and understanding of Tibetan Plateau dust emissions and transport, regional tectonics, and landscape dynamics as well as the potential climate and environmental implications.

1. Introduction

Aeolian dust exerts major impact on the global climate and has feedbacks with various components of the Earth's system, from the hydrologic cycle to the Earth's biosphere and atmospheric geochemistry. Moreover, this dust affects the Earth's radiation budget, thereby contributing to the acceleration of glacier melt, and has profound effects on the global biogeochemical cycles. Arid and semi-arid regions in Central and East Asia are among the world's largest dust sources (Chen et al., 2007; Maher et al., 2010; Osterberg et al., 2008; Uno et al., 2009; Wu

et al., 2010; Yang et al., 2007). More than 800 Gt of dust is estimated to be transported into the atmosphere every year, mainly from Asia (X. Y. Zhang. (2001); Prospero et al., 2002; Zhang et al., 2003). Several studies have shown that Asian dust is the major component of the Chinese loess deposits and makes up a significant component of dust deposition in Japan, Korea, Greenland, and the North Pacific (Bory et al., 2003; Chen et al., 2007; Pettke et al., 2002). The Tibetan Plateau (or Qinghai-Tibet Plateau, abbreviated to TP) region of Asia is one of the important sources of dust in the area and exerts significant influence on the East Asian summer monsoon (Fang et al., 2004; Mao et al., 2013, 2019; Sun et al., 2017). Recent studies have also shown that desertification is expanding the Tibetan Plateau's arid regions, so that dust production in the Tibetan Plateau shall become more intense in the years ahead (Dong et al., 2017, 2020).

The TP and its adjacent mountains, known as the Earth's "Third Pole", constitute a unique geographic unit that is associated with the highest elevation in the Earth's mid-latitude region. The collision between the Indian and Eurasian plates makes the TP one of the most active tectonic areas of the Earth. However, different regions of the TP respond to this collision in distinct ways, because of the spatial heterogeneity in the crustal properties and stress transfer inherent to the geologic system of the TP. Specifically, this spatial heterogeneity causes differences in the local time-scale and amplitude of uplift in response to the tectonic forcing applied (Mulch & Chamberlain, 2006; Royden et al., 2008; Tapponnier et al., 2001). During structural uplift, continuous exposure of fresh rock leads to denudation and fragmentation of the surface crust under the influence of earth-surface erosion processes (such as glacial erosion, weathering, etc.). The fine particles produced by physical-chemical weathering and erosion can enter, then, into atmospheric circulation, thereby affecting the climate both at regional and at global scale (Dong et al., 2016). However, there is still poor knowledge of the production and transport mechanisms leading to surface dust emission and deposits on the TP. The understanding of these mechanisms is important for a broad range of fields, given the profound feedbacks of Aeolian dust with geology and climate, and the need to improve our knowledge about the implications of Earth's changing climate for the dust dynamics.

Previous studies have shown that the $^{234}U/^{238}U$ isotope ratio of fine particles (smaller than 50 μm) reflects the time elapsed since their separation from bedrock (Bourdon et al., 2003, 2009; DePaolo et al., 2006, 2012; Lee et al., 2010). Moreover, particles that originated from different source areas are often associated with distinct fragmentation mechanisms, surface transport pathways, and, thus, comminution ages (Dou et al., 2016; Li et al., 2016; G. J. Li et al., 2017; Sun, 2005). Therefore, the distribution of the $^{234}U/^{238}U$ ratio – which is usually expressed as the ($^{234}U/^{238}U$) activity ratio, that is, a value corresponding to the equilibrium ratio – can be used to track particle source and age (DePaolo et al., 2006, 2012). This method, here referred to as uranium (U) comminution age method, can be also used to trace a series of intermediate phases such as dust production, transportation and deposition, and has been effectively applied as a new geological method in various applications involving deep-sea sediments (DePaolo et al., 2006), river sediments (Chabaux et al., 2012; Handley et al., 2013; Lee et al., 2010), lake sediments (Francke et al., 2020), glacial basins (DePaolo et al., 2012; Xu et al., 2019) and loess on the Chinese Loess Plateau (L. Li et al., 2017, 2018). Here we use the U comminution age method to obtain information about the origins of the surface dust in the TP region, including potential transport paths and erosion processes that led to the spatial distribution of surface dust in the area of investigation. Our study shall thus contribute to deepen the understanding of dust production and transport in the TP region, as well as of the geological processes underlying the landscape dynamics of the TP.

This work is the first to measure the ^{234}U and ^{238}U isotopic composition of surface dust particles in the cryospheric regions of the Tibetan Plateau and to use the U comminution age method to reveal the spatial variation of the ($^{234}U/^{238}U$) values and to infer the evolution processes of TP dust. Furthermore, we use the U isotopic composition of dust from several snowpack and cryoconite samples of glaciers in the TP to constrain TP dust transport distances and major sink areas both near and far. Cryoconite is a dark-colored and carbon-rich material consisting of mineral dust, microorganisms and algae, which deposits on the surface of snow, ice caps, and mountain glaciers (Dong et al., 2016; Stibal et al., 2012; Takeuchi & Li, 2008). Overall, the research provides new insights and understanding of TP dust emission and transport, regional tectonics, and landform dynamics, as well as the potential climatic and environmental implications.

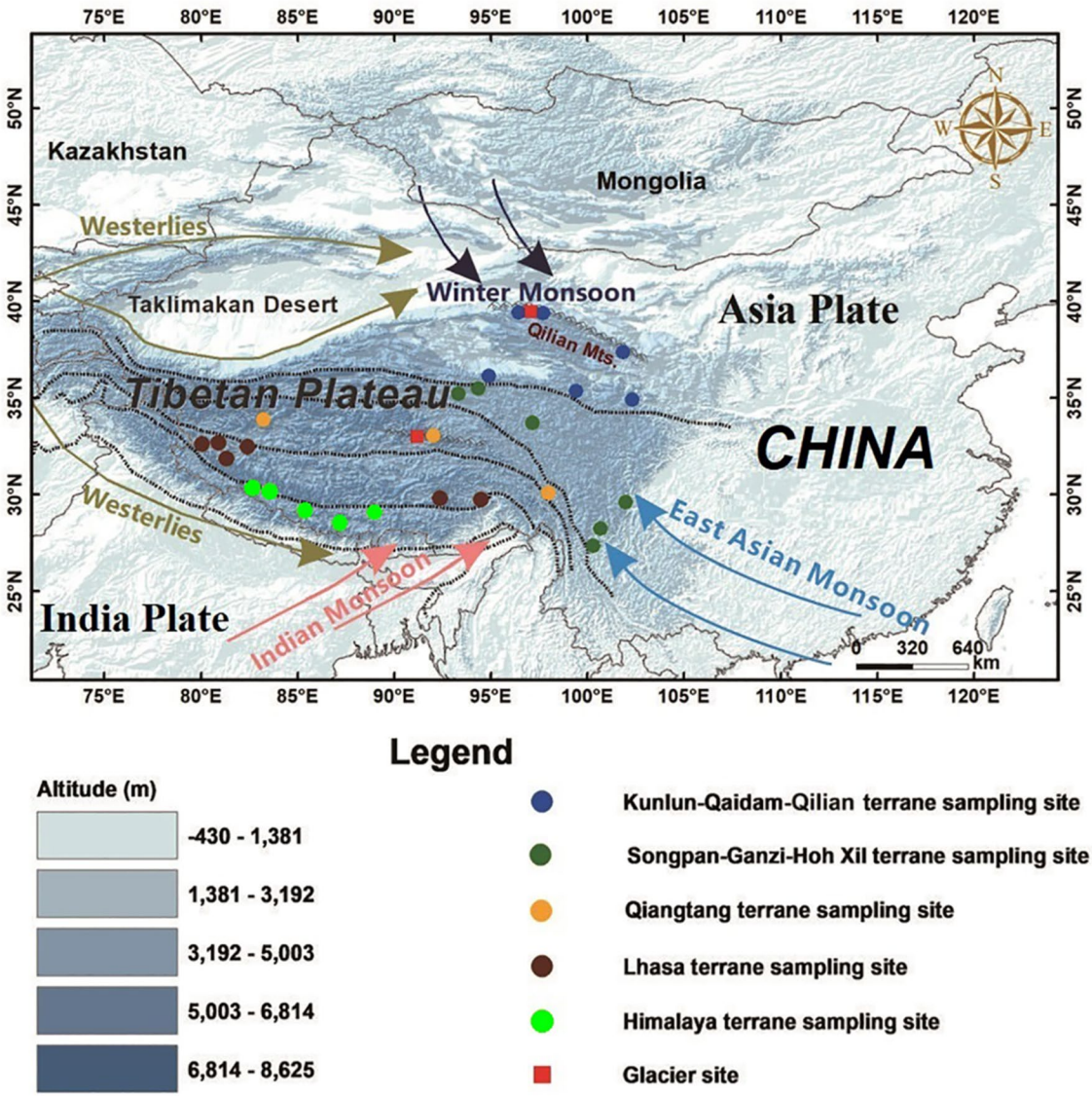

Figure 1. Location map showing the study areas and the sampling sites of the Tibetan Plateau dust, including the samples from Himalaya terrane (laurel-green), Lhasa terrane (claret-red), Qiangtang terrane (orange), Songpan-Ganzi-HohXil terrane (dark-green), and Kunlun-Qaidam-Qilian terrane (navy blue). The division of the terrane is based on Chen et al. (2017) and the climatic regionalization is referred from Dong et al. (2020).

2. Materials and Methods

2.1. Field Sample Collection

A total of 26 surface dust samples and three glacier snowpack/cryoconite dust samples were collected from various locations in different terranes across the Tibetan Plateau (25–40°N, 74–104°E; see Figures 1 and 2), including five samples on the Himalayan terrane, six samples of the Lhasa terrane, three samples in the Qiangtang terrane, six samples in the Songpan-Ganzi terrane and six samples of the Kunlun-Qaidam-Qilian terrane, to find out the regional U isotopic variation of the TP surface dust samples. The upper 5 cm of surface dust was collected with a trowel and stored in precleaned, low-density polyethylene bottles (Thermo Scientific), by removing the top 1 cm of topsoil. In addition, the U isotopic composition of snow/glacial dust samples collected from two glaciers in the northern TP (Laohugou Glacier No.12 and Dunkemadi Glacier), were used to compare and analyze the sources of surface dust deposition on high-altitude glaciers, so as to constrain the transport distances of Tibetan dust.

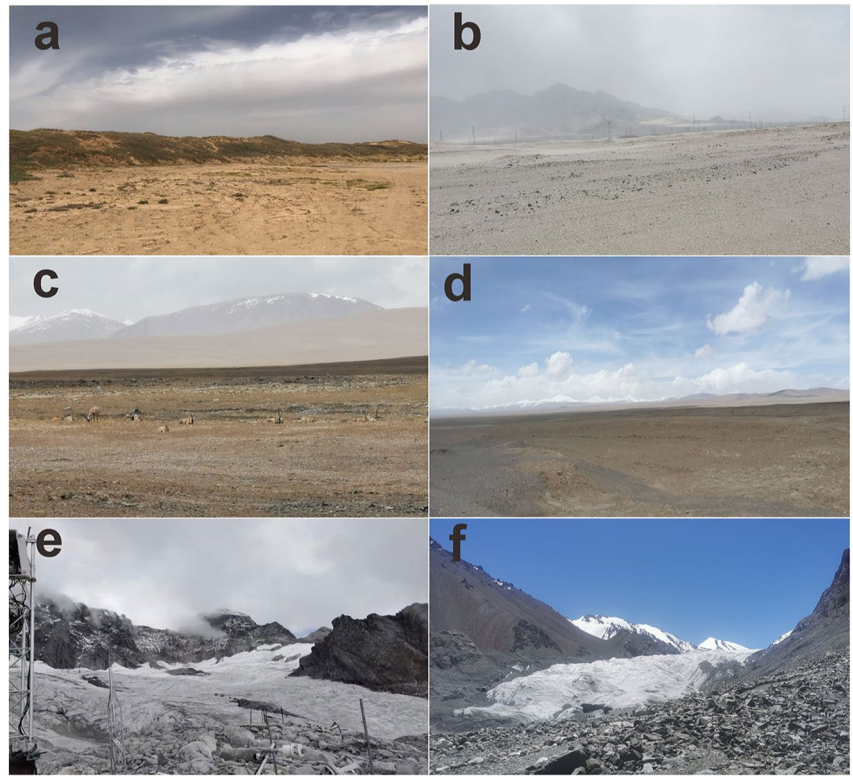

Figure 2. Photo shows the background geomorphology and geological information of the sampling locations. The geomorphic environment of the sample sampling sites were all selected in the flat area on the plateau, except for several points in the glacier area where erosion and fragmentation strongly transported but still belonged to the local mixed influence, which could reflect the intense erosion and particle fragmentation process in the glacier area.

We remark that all samples investigated in the present work are surface dust samples, that is, the dust on the soil to form unconsolidated sediment with no structure. In particular, the TP surface dust samples were derived from the surface of arid regions in the TP, where aeolian dust emission is an important environmental process (Dong et al., 2017; Fang et al., 2004; Han et al., 2009). We thus refer to these samples as "TP dust". Aeolian dust particles can be transported through the atmosphere, thereby constituting an important agent for the Earth's climate. Indeed, dust particles transported from different regions within the Tibetan Plateau may reflect valuable information about geological and climatic aspects of their respective sources, as we specify next. The samples of north TP were collected in the Qilian and Kunlun Mountains, which comprise an area affected both by uplift processes in the Plateau and by the East Asian winter and summer monsoon systems. Moreover, the Himalayan orogenic belt in the south TP is one of the key areas that can provide information on the formation and evolution of the TP (Aitchison et al., 2000; Decelles et al., 2000; Xu et al., 2019), while the southeast TP includes the central and northern section of the Hengduan Mountains and the eastern section of the Yarlung Zangbo River Basin. This region has been subjected to very strong tectonic activities under the impact of the plate collision since the Cenozoic era (Deng et al., 2015; Ouimet et al., 2010). Furthermore, the western TP is also a hotspot for the study of the early geological evolution of the TP (Jin et al., 2003; Zheng et al., 2006). Therefore, the surface dust samples locations selected in this work reflect the TP's spatial extent. Based on the samples collected from these locations, the aim of our study is to acquire additional information that will shed further light on the tectonic evolution and climate of the region as well as information on dust source tracking. The relevant information about the samples and their respective locations is provided in Table 1.

2.2. Mineral Composition Analysis

TP dust was subjected to an X-ray fluorescence spectroscopic analysis (XRF) using a Arladvant 'x IntellipowerTM3600 scanner. Based on this analysis, we conclude that the composition of clay-sized (<5 μm) and

Table 1
Information of the Sampling Locations of Surface Soil and Snowpack/Cryoconite Dust in the Tibetan Plateau

Sample No.	Latitude (°N)	Longitude (°E)	Elevation(m)	Sample type	($^{234}U/^{238}U$)	2SD	ε_{Nd}[a]	$^{87}Sr/^{86}Sr$[b]
Himalaya terrane								
TP1850	29.32	85.21	4,471	Surface soil	0.977	0.002	−14.3	0.72601
TP1836	29.29	88.9	3,833	Surface soil	0.960	0.003	−14.3	0.72625
TP1854	30.54	82.56	4,911	Surface soil	0.990	0.003	−14.2	0.72424
TP1844	28.51	87.07	5,182	Surface soil	1.007	0.004	−16.1	0.72732
TP1862	32.43	80.21	5,007	Surface soil	1.009	0.002	−13.5	0.72760
Kunlun-Qaidam terrane								
TP18117	35.41	99.43	3,241	Surface soil	0.956	0.002	−11.5	0.72254
Luqu	34.58	102.48	3,500	Surface soil	0.960	0.003	−10.5	0.72129
Yuzhufeng3	35.71	94.28	4,374	Surface soil	1.026	0.002	−10.9	0.72281
Qiyi	39.38	97.63	3,883	Surface soil	0.991	0.002	−10.8	0.72102
Hulugou1	37.5	101.92	3,497	Surface soil	0.983	0.002	−9.5	0.71952
LHG	39.5	96.52	4,450	Surface soil	0.997	0.003	−10.1	0.72102
Qiangtang terrane								
TGL	33.04	92.05	5,714		0.964	0.002	−13.5	0.72281
HjS13	33.57	83.7	3,277	Surface soil	0.968	0.002	−12.1	0.72210
TP1898	30.06	97.98	2,860	Surface soil	0.972	0.002	−13.1	0.72250
Lhasa terrane								
TP1886	29.46	94.53	2,913	Surface soil	0.965	0.002	−12.9	0.72622
TP1884	29.83	92.34	4,386	Surface soil	0.968	0.002	−14.3	0.72851
S5	31.58	81.18	3,132	Surface soil	0.973	0.002	−14.2	0.72013
S2	32.3	82.31	2,979	Surface soil	0.954	0.003	−13.1	0.72013
HjS25	32.5	80.2	3,140	Surface soil	0.962	0.002	−13.5	0.72124
HjS32	32.4	80.1	2,850	Surface soil	0.952	0.002	−13.8	0.72124
Songpan-Ganzi-Hoh Xil terrane								
TP1812	35.91	94.7	4,450	Surface soil	0.998	0.002	−9.7	0.72281
TP1815	35.3	93.3	3,445	Surface soil	0.993	0.003	−9.7	0.72281
TP18114	33.79	97.15	3,423	Surface soil	0.956	0.002	−11	0.72632
Gongga2	29.59	101.89	3,136	Surface soil	0.996	0.004	−15.1	0.72524
Daocheng	29.04	100.31	3,900	Surface soil	1.008	0.004	−15.3	0.72311
YL	27.1	100.1	3,400	Surface soil	1.001	0.002	−14.2	0.72390
Glacier								
LHG29-4	39.5	96.52	4,450	Snowpack	0.965	0.002	−9.5	0.72153
LHG30-1	39.5	96.52	4,450	Cryoconite	0.999	0.002	−10.5	0.72208
TGL19-19	33.04	92.05	5,714	Snowpack	0.966	0.002	−12.5	0.72510

[a]Nd isotope data references from Wei et al., 2021. [b]Sr isotope data references from Wei et al., 2021.

coarser-sized (5–100 μm) dust minerals (Figure S1 in Supporting Information S1) in the study area of TP is mainly silicate. Illite (mainly SiO_2, Al_2O_3, and Na_2O) is the dominant mineral, accounting for more than 70% of the total content, followed by chlorite (mainly composed of SiO_2, Fe_2O_3) and kaolinite (composed of SiO_2, Al_2O_3, K_2O, Na_2O and CaO), with negligible montmorillonite content. Illite is a layered clay mineral similar to mica (mainly SiO_2, Al_2O_3, H_2O; Table S1 in Supporting Information S1), is formed mainly by weathering of muscovite or potash feldspar, and can undergo chemical modification thus giving rise to other clay minerals. Furthermore, common clastic minerals are quartz, feldspar and iron. A previous study also indicated similar results for the

mineral composition in the TP surface soils (Y. Li, 2014). The characteristics of mineral composition indicate that the study area of TP is characterized by a dry and cold climate dominated by physical weathering and weak chemical weathering (Wei et al., 2021).

Moreover, we also performed a laboratory analysis of mineral composition using an X-ray diffraction (XRD) equipment (Panalytical X'Pert PRO), which combines an X-ray tube working voltage of 40 kV with a tube current of 250 mA. Quantitative analyses of the minerals were performed using the Rietveld method. Specifically, by applying this method, we use the X-ray diffraction patterns of the dust samples to determine the material structure based on the height, width and position of the peaks in intensity of the diffraction patterns (Jin et al., 2021). The results of these analyses, that is, the proportions of the different materials constituting the samples, were normalized to 100% based on the assumption that the mineral contents of the samples were entirely accounted for by the XRD patterns.

2.3. Comminution Analysis of the Uranium Isotopes

Comminution analysis is based on the recoiling effect during alpha (α) decay of ^{238}U. The ^{234}U in the rock is the product of ^{238}U undergoing one α decay to ^{234}Th and then undergoing two β decays. The unstable ^{234}U continues to undergo α decay to become ^{230}Th. After a number of U series decays (about 1 Ma), the U isotope in the bedrock will reach a state of equilibrium, that is, the production rate of ^{234}U is equal to the decay rate of ^{234}U:

$$\lambda_{238} \cdot {}^{238}U = \lambda_{234} \cdot {}^{234}U \tag{1}$$

in the equation above, λ_{234} denotes the decay constant of ^{234}U, and amounts to, approximately, of 2.82206×10^{-6}/a, while λ_{238} is the decay constant of ^{238}U (L. Li et al., 2017), which has an approximate value of 1.55125×10^{-10}/a. Since the absolute ratio of ^{234}U/^{238}U is very small, it is usually expressed as the radioactivity ratio (^{234}U/^{238}U):

$$({}^{234}U/{}^{238}U) = \frac{\lambda_{234} \cdot {}^{234}U}{\lambda_{238} \cdot {}^{238}U} \tag{2}$$

under initial equilibrium conditions, the value of (^{234}U/^{238}U) is equal to 1. Such a secular equilibrium is disturbed when fine particles (≤50 μm) are generated because a significant portion of ^{234}U is ejected out of the particle due to the recoil effect during α-decay of ^{238}U, thereby rendering the ^{234}U accumulation rate of particles lower than the decay rate (DePaolo et al., 2006; L. Li et al., 2017). Therefore, the (^{234}U/^{238}U) decreases gradually with time from the onset of comminution, until the new steady-state equilibrium is reached. The value of (^{234}U/^{238}U) provides thus a proxy for the time elapsed from dust generation, including intermediate processes between comminution and deposition.

To conduct the analysis, the surface dust samples were first immersed in 0.5 mol/L acetic acid for 2 hr to disperse and remove the carbonate fraction. The dispersed samples were then processed with an electroforming sieve to separate particle sizes with a diameter of 10–50 μm from the sample. This step is necessary because the principle is that the decrease in the ^{234}U content of clastic fine particulate matter is caused by the recoil effect. More precisely, once the rock is broken down, the ^{234}U will be continuously lost from the thin outer particle layer due to alpha recoil, following ^{238}U decay and ejection of ^{234}Th (the precursor to ^{234}U as discussed above). Overall, this process results in a reduction of ^{234}U accumulation. However, owing to limitations associated with the instrument resolution, the ratio change of ^{234}U/^{238}U can be detected only when the particle size is small enough (usually $d \leq 50$ μm; DePaolo et al., 2006; Lee et al., 2010). Importantly, the uncertainty of particle comminution time caused by particle size can be effectively reduced as long as the particle size is controlled within a certain range (see Lee et al., 2010).

Usually, fine particles move out of equilibrium faster than larger particles. However, this principle varies appreciably only within a certain grain size range. Therefore, the particle size distribution of TP dust was measured (mainly dust, with particle size range of 0.5–200 μm of >90% particles in number, as shown in Figure S1 in Supporting Information S1) using an Accusizer 780A (Thermo Fisher), and samples with a particle size range of 10–50 μm were selected for U comminution age method analysis. Within such a particle size range, the U isotope comminution age fits within the ideal range (DePaolo et al., 2006, 2012) and reflects the overall trend of the (^{234}U/^{238}U) value, which decreases with increasing.

After sieving, the samples were first reduced and cleaned to remove the adsorbed iron-manganese oxides, hydroxides, and other non-detritus materials. Here we referred the pre-treatment method of dust samples in the previous study, as follows: (a) The carbonate minerals were first removed by soaking dilute acetic acid solution (0.5 mol/L) at room temperature for 2 hr; (b) The second step is to remove iron and manganese oxides and hydroxides were removed by using one-time sodium bicarbonate –sodium citrate –sodium hyposulfite reduction soaking; (c) Then, organic matter was removed with 5% hydrogen peroxide solution at 85°C (L. Li et al., 2017). This process has proven effective in removing the influence of non-detrital material ($^{234}U/^{238}U$) values, so as to obtain the lowest ($^{234}U/^{238}U$) value. Our results also eliminate the influence of non-detrital material to the maximum extent as detected in the laboratory.

The pre-treatment for the removal of the oxides and organic matter was concluded in the ultra-purification analysis laboratory of the State Key Laboratory of Cryosphere Science in Lanzhou, China. HF-HNO_3 was then used to digest the silicate minerals and we used UTEVA resin to separate the U element. U isotopic ratios were measured by means of a Plasma II multi-collector inductively coupled plasma mass spectrometer in the Analysis Center of Beijing Institute of Geology of the Nuclear Industry, in which ^{238}U is collected within a Faraday cup, while ^{234}U is collected by a secondary electron multiplier. Furthermore, the Standard Sample Bracketing method was used to correct the short-term variation of the instrument (L. Li et al., 2017). Instrumental bias between ^{234}U and ^{238}U was corrected by normalizing the $^{238}U/^{235}U$ ratio to 137.84. The long-term measurement result of the international standard USGS BCR-2 reference material ($^{234}U/^{238}U$) is 1.001 ± 0.003 (n = 20, 2σ), which is consistent with the internationally recognized ratio within the error range. For the measurement of ($^{234}U/^{238}U$) in snowpack and cryoconite dust samples, we refer to the previous work by Aciego et al. (2009).

3. Results

3.1. U Isotopic Composition of Tibetan Plateau Dust and Its Geospatial Distribution

In this work we divide the sampling area of U isotopic composition into different subareas from north to south, based on the geological terranes of the TP (such as Chen et al., 2017; i.e., the distribution of sutures and terranes on the TP). These subareas from north to south are: the Kunlun-Qaidam-Qilian terrane, the Songpan-Ganzi-Hoh Xil terrane, the Qiangtang terrane, the Lhasa terrane and the Himalayan terrane (see Figures 1 and 3), respectively. Figure 1 shows detailed separation of the sampling sites based on the geological units (terranes) of the TP. Moreover, Figure 3 shows the geographical locations associated with our measurements and also the geospatial variation of ($^{234}U/^{238}U$) values of TP dust. We find that the spatial variation in U isotope of TP dust becomes more evident by dividing the area into the subareas indicated in Figures 1 and 3, that is, reflecting the distinct geology of the various terranes. Overall, the Songpan Ganzi-Hoh-Xil terrane shows the highest value of ($^{234}U/^{238}U$), with an average of 0.992 ± 0.018. While the samples collected from the Himalayan terrane in the south TP and the Kunlun Qaidam terrane in the north TP displayed mean ($^{234}U/^{238}U$) values of 0.988 ± 0.021 and 0.986 ± 0.026, respectively, and the mean value of this quotient was 0.968 ± 0.004 for the samples from Lhasa terrane, and 0.962 ± 0.008 for the samples of Qiangtang terrane in the central TP. The spatial variation of the ($^{234}U/^{238}U$) isotope ratios of TP dust showed that relatively high values appeared in the Songpan-Ganzi-Hoh Xil, Himalayan and the Kunlun-Qaidam-Qilian terranes. Moreover, the ($^{234}U/^{238}U$) values were rather low in the Lhasa and Qiangtang terranes. However, among all samples the highest value occurred in the glaciation zone, where sediments are relatively young (e.g., north TP; see Table 1 and Figure 3b).

The Kunlun-Qaidam-Qilian terrane in north TP is located in the East Kunlun fault zone, where the geological structure is complex and tall mountains and basins are intricately distributed. The high-relief topography and numerous glacial landforms are present above the altitude of 4,300–5,000 m. a.s.l. In this study, the U isotope values of local dust samples from Yuzhufeng Glacier area of the Kunlun Mountains (1.026), Qiyi Glacier (0.991) and Laohugou Glacier (0.997) area of the Qilian Mountains are relatively high.

Moreover, the Songpan-Ganzi-Hoh Xil terrane located in the central and northern TP has the most flat terrain in the whole TP (Figure 1), and the block is relatively stable inside (Li et al., 2021). However, the eastern boundary is mainly characterized by compressive deformation, and the geological structure is active, with earthquakes occurring frequently in the eastern region of the terrane. Thus, the ($^{234}U/^{238}U$) values of dust samples near the boundary zone of this terrane (e.g., the samples TP1815, TP1812, Daocheng, YL, and Gongga derived

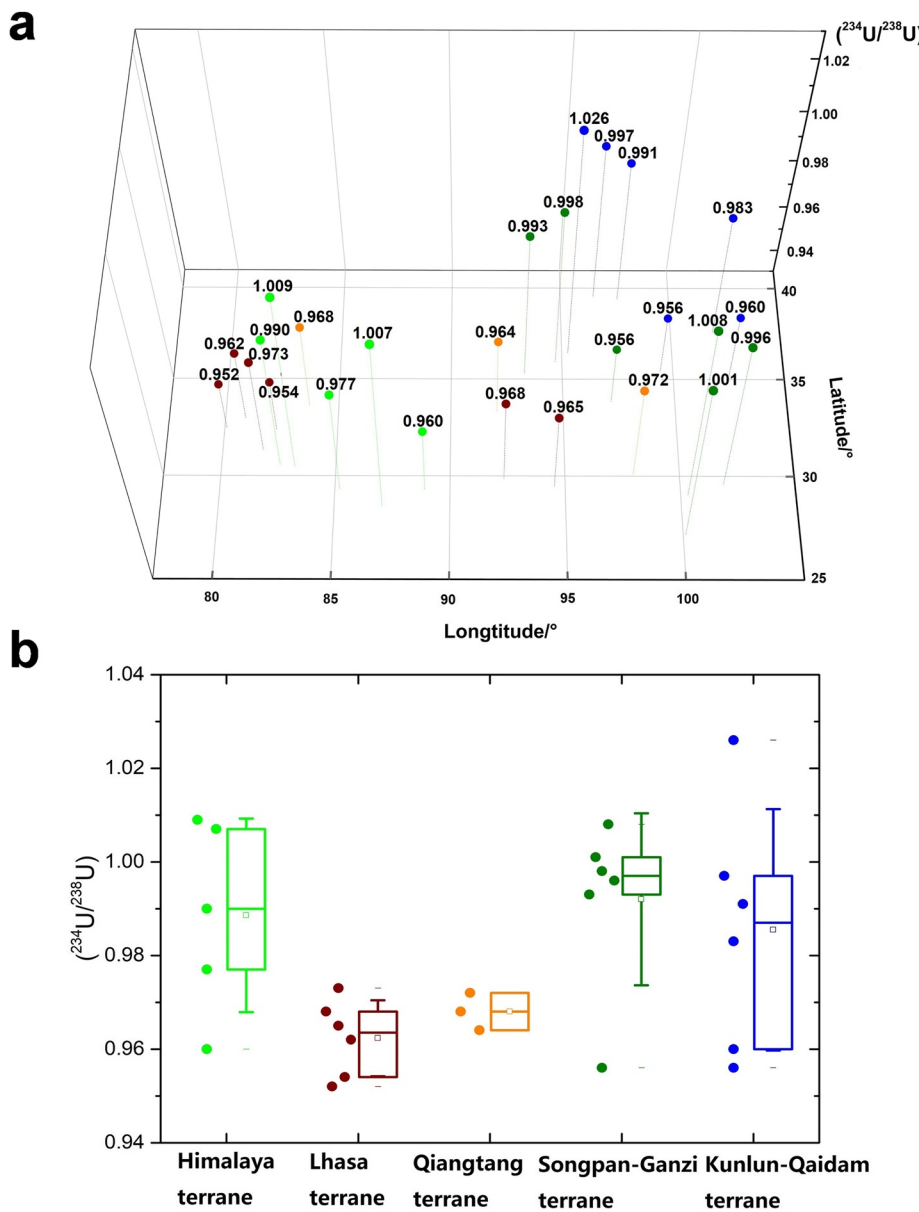

Figure 3. ($^{234}U/^{238}U$) values of surface soil in various terranes of the Qinghai-Tibet Plateau (a) and their geographic distribution (b). Different colors represent the ($^{234}U/^{238}U$) values of samples separation with different terrane, including the Himalaya terrane (laurel-green), Lhasa terrane (claret-red), Qiangtang terrane (orange), Songpan-Ganzi-HohXil terrane (dark-green), Kunlun-Qaidam-Qilian terrane (navy blue). The rectangles indicate the upper and lower quartiles and the median is shown as a horizontal line, the squares of different colors within the boxes refer to the arithmetical mean (3b).

in the Hengduan Mountains) have much higher values, while the samples located in the interior part show lower ($^{234}U/^{238}U$) values (e.g., TP18114, Figure 3b).

The Qiangtang terrane in the hinterland of TP is characterized by a topography of low hills and wide valleys in lake basins. This terrain is gently undulating, and constitutes an area with early geological uplift and a well-preserved planation surface of the TP (Y. L. Li et al., 2015). The Tanggula Mountains, the boundary between the north and south TP, is located here. This region has not been affected by fluvial erosional processes caused by the strong uplift of the plateau, so the terrain in this region is gently undulating, with early geological uplift and a well-preserved planation of the plateau (Y. L. Li et al., 2015; Pan et al., 2009).

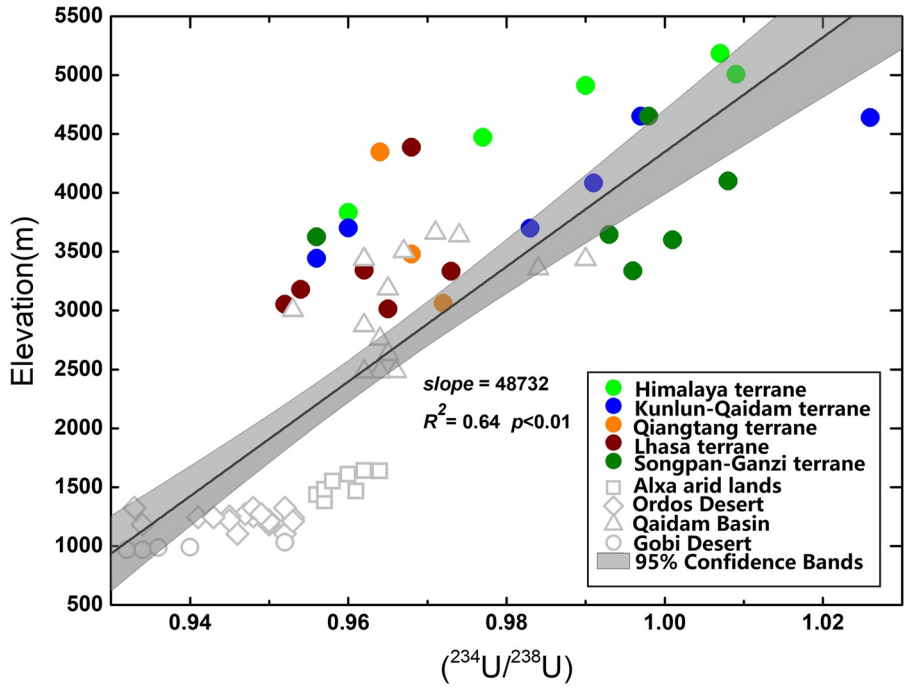

Figure 4. Correlation between ($^{234}U/^{238}U$) isotopic ratios and elevation of the surface dust in the Tibetan Plateau, Alxa arid lands, Ordos Desert, Gobi Desert and Qaidam Basin, which showed good correlation between the U isotopes and elevation ($R^2 = 0.64$). The dark gray area is the range of the fitted 95% confidence interval. The colored circles represent the surface soils of the Tibetan Plateau, and the gray hollow shapes represent data obtained from the literature (Li et al., 2018).

The southern TP comprises the Lhasa and Himalayan terranes where the landscape is very undulating (Y. L. Li et al., 2015; Xu et al., 2006), and the boundary between them is the Yarlung Zangbo suture zone, with an average elevation from 4,600 m to 6,000 m a.s.l. Due to the great collision between the Indian and the Eurasian plates, the southern TP is constantly uplifted and the Yarlung Zangbo River basin was compressed northward, forming a deep and large fault structure with approximately east-west direction and Yarlung Zangbo suture zone. The tectonic activity is extremely active and faults crisscross each other. Therefore, neotectonic movement has a fundamental impact on the terranes of this region (Y. L. Li et al., 2015; Yin, 2006). In this study, the surface dust sampling of the Lhasa terrane was concentrated in relative flat areas (such as the gently topographic valley around Lhasa and the plateau in Ngari area), which explain the low ($^{234}U/^{238}U$) values obtained for the Lhasa terrane. By contrast, the Himalayan terrane samples were collected from the Himalayan foothills and surrounding mountains, and the tectonic activity is high with high rates of modern weathering and erosion processes, comparable to the value of ($^{234}U/^{238}U$) of the Kunlun-Qaidam-Qilian terrane and eastern Songpan-Ganzi-Hoh Xil terrane where the terrain is rather rugged.

3.2. U Isotope Change With the Elevation of Sampling Locations in Tibetan Plateau

Figure 4 indicates the correlation between ($^{234}U/^{238}U$) values and elevation. The ($^{234}U/^{238}U$) activity ratios showed a strong and significant linear correlation ($R^2 = 0.64$, $p < 0.01$) with increase in elevation (Figure 4). The ($^{234}U/^{238}U$) values on the inner plateau's flat surfaces are relatively low, which is in sharp contrast to the high isotope values of the samples in the glaciated area and the region with increased mass wasting in high mountains, such as Himalaya and Kunlun Mountains. The samples with higher ($^{234}U/^{238}U$) values were derived from the glacial areas of Yulong Snow Mountain Glacier and Hailuogou Glacier of the Hengduan Mountains in southeast TP, Laohugou Glacier No.12 (in the Qilian Mountain) and Yuzhufeng Glacier (in the Kunlun Mountains) of the northern TP, and the Himalayan foothills in south TP.

3.3. Mineral Composition of Tibetan Plateau Surface Dust

Moreover, XRD and XRF measurements showed that the mineral composition of TP dust is nearly the same for all sampling locations (Tables S1 and S2 in Supporting Information S1). The results showed that the mineral composition of dust on the Tibetan Plateau does not vary much over the different locations, consisting mainly of quartz, K-feldspar, plagioclase, calcite, muscovite and clay minerals (Figure S2 in Supporting Information S1). Here we found that the mineral composition of TP dust is generally similar over the various sampling locations, based on the XRF and XRD measurements of mineral composition (Tables S1 and S2, Figure S2 in Supporting Information S1). The composition of clay-sized and coarser-sized dust minerals in the study area of TP is mainly silicate (Table S1 and Figure S2 in Supporting Information S1). Illite (mainly composed of SiO_2, Al_2O_3, and Na_2O) is the dominant mineral, accounting for more than 70% of the total content, followed by chlorite (mainly composed of SiO_2, Fe_2O_3) and kaolinite (composed of SiO_2, Al_2O_3, K_2O, Na_2O and CaO), which basically contain no montmorillonite. Both the oxide and mineral compositions showed high similarity for samples from all the locations (see Figure S2 and Tables S1, S2 in Supporting Information S1). Our XRF measurements showed that SiO_2 has the highest concentration among all the oxide components (with high Si element content) in each site, followed by Al_2O_3 and CaO. Furthermore, our XRD measurements also showed that quartz, chlorite, calcite and biotite are the major minerals for dust samples in all Tibetan sites.

4. Discussion

4.1. Factors Influencing U Isotopic Composition and Spatial Distribution

Compared to the ($^{234}U/^{238}U$) values of TP dust and other sediment deposits worldwide, the ($^{234}U/^{238}U$) values of fluvial sediments in various river basins around the world are high (Figure 5 and Table 2). For example ($^{234}U/^{238}U$) values of the Murray-Darling Basin sediments fall within the range 0.975–1.06 (Dosseto, Turner & Dougles, 2006), while for the Himalayan river sediments these values are between 0.995 and 1.032 (Granet et al., 2007). Moreover, the sediments in the Amazon River basin have values of ($^{234}U/^{238}U$) in the range (from 0.979 to 1.033; Dosseto, Bourdon et al., 2006). These values are higher than the ($^{234}U/^{238}U$) ratio associated with aeolian dust sink areas such as loess sediments in Chinese Loess Plateau (0.897–0.960; L. Li et al., 2017, 2018), lake sediments (0.9–1.006; Francke et al., 2020), deep-sea sediments (0.83–0.97; DePaolo et al., 2006) and ice core dust (0.88–0.99; Lupker et al., 2010). The ($^{234}U/^{238}U$) values of high-altitude mountains and glaciated areas tend to be the highest due to short comminution and transport time, whereas dust end-members (sediments) showed relatively lower values with long–term transport and comminution. Previous study has indicated that the basin draining Himalayan rivers is located in an active tectonic zone with high relief that produces plenty of fresh comminuted particles, which can then be quickly transported (Granet et al., 2007). Moreover, Iceland is heavily glaciated and tectonically active, which can rapidly erode the surrounding rocks and supply large quantities of detrital particles with high ($^{234}U/^{238}U$) values (Vigier et al., 2006).

The ($^{234}U/^{238}U$) values of TP dust (0.952–1.026) are located between the range of values obtained from river sediments and the values from some dust deposition sinks (such as loess). The higher value of fluvial sediments is attributed to the faster transport time and shorter transport distance of sediments in alpine environments, whereas the lower value of loess is due to the longer residence time after deposition. Therefore, the ($^{234}U/^{238}U$) values of TP dust may be understood from the mixing of particles with short comminution time – associated with geotectonic processes, glacial erosion, and landscape dynamics (mass wasting) –, and particles with long residence time on the plateau surface. TP is a large tectonic geomorphic unit formed by a large-scale, staged and uneven fault-block uplift process that has been occurring since the Late Cenozoic (Chung et al., 1998; Harrison et al., 1992; J. J. Li et al., 2015; Tapponnier et al., 2001; Zheng & Zhao, 2017). Therefore, the tectonic evolution and landform dynamics of the terranes vary regionally. Correspondingly, the fine particulate materials deposited on the surface of the different terranes considered here are associated with very different ($^{234}U/^{238}U$) activity ratios. The spatial variation of the ($^{234}U/^{238}U$) isotope ratios of TP dust showed relatively high values in the Songpan-Ganzi-Hoh Xil, Himalayan and the Kunlun-Qaidam terranes, as well as relatively low ($^{234}U/^{238}U$) values in Lhasa and Qiangtang terranes. However, among all samples the highest values appeared in the glaciation zone (e.g., northern TP), thereby reflecting influence of regional tectonic evolution, landscape dynamics and glacial erosion processes.

In order to determine the general variation of U isotope among different terranes and the relationship between U isotope and plateau surface evolution, most of the TP dust samples were collected in relatively flat areas of

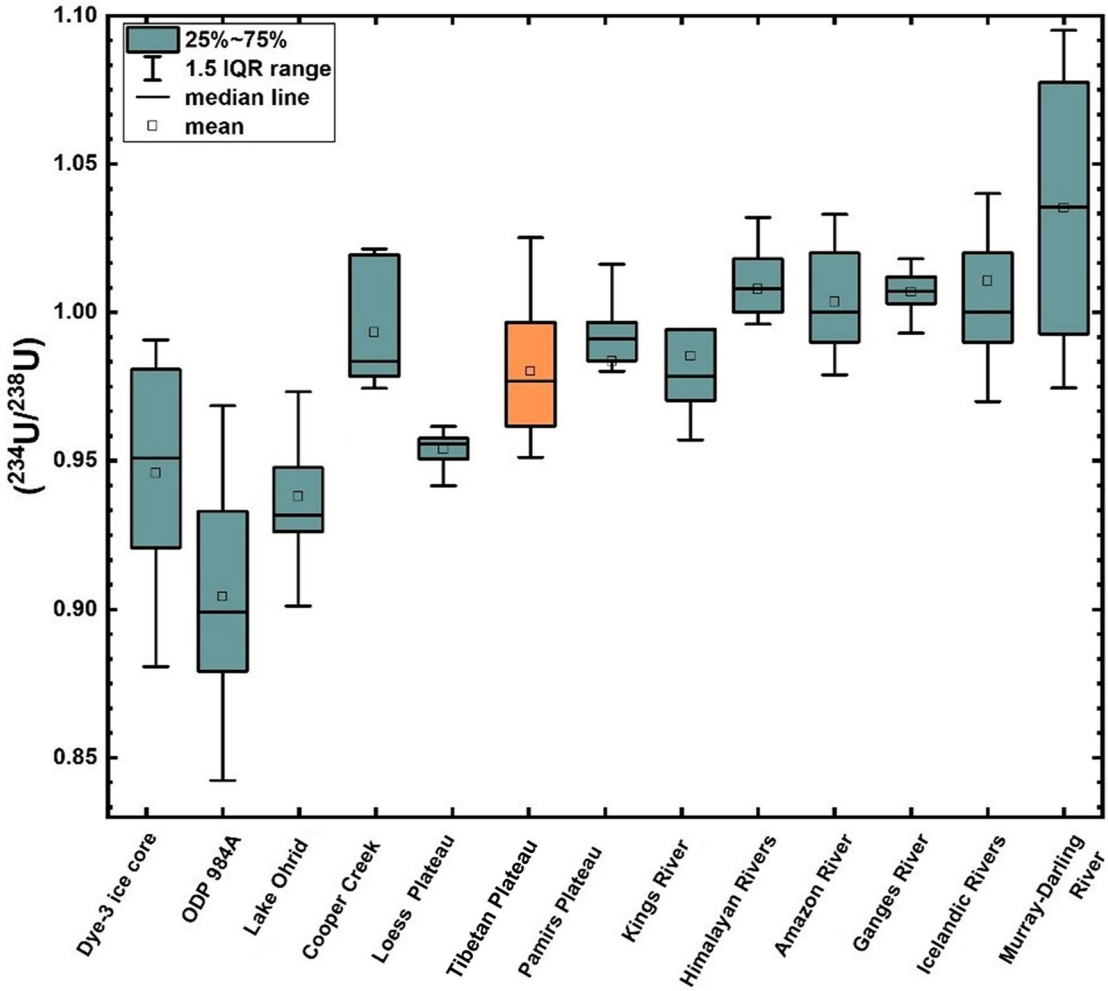

Figure 5. Comparison of ($^{234}U/^{238}U$) values in the Tibetan Plateau (the yellow box) with different types of sediments such as river sediments, Greenland ice cores, deep sea and lake sediments, and loess on the Loess Plateau in China (Chabaux et al., 2012; DePaolo et al., 2006; Dosseto, Bourdon et al., 2006; Dosseto, Turner & Douglas, 2006; Francke et al., 2020; Granet et al., 2007; Lee et al., 2010; L. Li et al., 2017; Lupker et al., 2010; Vigier et al., 2006; Xu et al., 2019).

each plateau region (Figure 2), and others were collected from the glaciation zone, high-relief mountain range, and only very few were collected from the river valley (e.g., the sample TP1844, dry surface dust but far away from river sediments). Stratified landforms (such as planation and denudation surfaces) are important as proxy for the uplift and surface evolution of the Tibetan Plateau (J. J. Li et al., 2015; Pan et al., 2004). A planation surface, representing the final stage of landform development, is formed at a low altitude, with little relief and slow surface material migration. The TP has undergone several planations in geological history (Liu et al., 2015; Pan et al., 2004). The main planation surface of the plateau may represent the result of geomorphic erosion cycle (Haider et al., 2013; Wang et al., 2012). Therefore, the lower ($^{234}U/^{238}U$) values of dust samples retained in the main part of the plateau may indicate the long term weathering and erosion of material. However, the higher values ($^{234}U/^{238}U$) in the samples may record fresh broken clastic sediments from modern tectonic evolution and surface erosion processes, which have a short comminution time and were quickly transported and deposited. Moreover, the geomorphic setting of the samples is also important for the U comminution age analysis, as a small part of the samples were collected in the glacier areas and other rugged landscapes (e.g., the samples from the Himalayas and Hengduan Mountains, and the Laohugou Glacier basin). This small part of the samples could reflect the intense erosion and particle comminution process and induced U isotope change.

Table 2
Comparison of U Isotopic Composition With Different Types of Sediment Media at the Global Scale

Location	($^{234}U/^{238}U$)	Sample type	References
Himalayan Rivers	0.995–1.032	Bedload or bank river sediments	Granet et al., 2007
Cooper Creek	0.978–1.021	Palaeochannel sediments	Handley et al., 2013
Ganges River	0.993–1.018	Suspended and bedload or bank river sediments	Chabaux et al., 2012
Pamirs Plateau	0.913–1.017	Surface sediments	Xu et al., 2019
Kings River	0.955–1.084	Alluvial fan sediments (bulk sample)	Lee et al., 2010
Amazon River	0.979–1.033	Suspended sediments	Dosseto, Bourdon, et al., 2006
Murray-Darling River	0.975–1.06	Suspended sediments (>25 μm)	Dosseto, Turner, & Douglas, 2006
Lake Ohrid	0.900–1.006	Lacustrine sediments	Francke et al., 2020
Dye-3 ice core	0.880–0.990	Ice core dust	Lupker et al., 2010
Ocean Drilling Program Site 984A	0.830–0.969	Deep-sea sediments	DePaolo et al., 2006
Icelandic Rivers	0.970–1.090	Suspended and bedload sediments	Vigier et al., 2006
Chinese Loess Plateau	0.897–0.960	Loess sediments	L. Li et al., 2017; Li et al., 2018
Tibetan Plateau	0.952–1.026	Surface soil	This study

From the above results we can conclude the possible influencing factors of U isotopic spatial variation.

(a) **Tectonic activity**. Tectonic activity has the most fundamental influence on the evolution of surface soil environment and, thus, on the surface dust fragmentation and its U isotope of the TP. The GPS velocity field observation in northern TP (Kunlun-Qaidam terrane) showed that the terrane surface is characterized by continuous deformation, consistent with the basin-range geomorphic structure formed by the deformation of the upper crust (Zhang et al., 2007). Basin-range structures formed by a series of thrust faults are developed, mainly with large terrain fluctuations. Intense glacial erosion and the marked differences in topographic relief configurations enable rapid transport of clastic material once denuded (Owen et al., 2006; Wu et al., 2001). Moreover, tectonic activity and the resulting topographic relief result in continuously exposed fresh rocks, which could provide a large amount of fresh clastic material with high ($^{234}U/^{238}U$) values. Differential uplift of mountains in this region also facilitates the timely removal of mechanical weathering products, thus continuously providing debris with short fragmentation time (Pan et al., 2009). Moreover, the Songpan-Ganzi terrane in central and northern TP showed a clockwise rotation from west to east. The overall slip rate does not change much at present, thus reflecting the characteristics of the overall quasi-rigid block moving to the east. The terrain around the block is clearly undulating, especially on the eastern margin, with horizontal shortening and vertical thickening of the upper crust (Liu et al., 2019). Furthermore, the GPS velocity field shows that there is no large-scale rapid slip in western Qiangtang block, while the eastern part display clear rapid migration, characterized by the rigid block movement of the whole material migration (Gan et al., 2007; Wang et al., 2001). The terrain in this eastern part is relatively flat with small fluctuations. However, in the southern TP (the Himalaya and Lhasa Terrane), the GPS velocity field shows significant S-N trending contraction and E-W trending extension, while the southern part of the TP has a strong E-W trending extension since the late Quaternary (Chevalier et al., 2020; Wang et al., 2017). Here, the terrain is highly undulating and the southern boundary thrust belt is frequently seismogenic. Overall, the intensity of tectonic activities is closely related to the weathering and denudation of rock particles, which fundamentally results in certain spatial differences of U isotopes in the sampling areas of various platforms on the TP.

(b) **Bedrock lithology**. The relationship between U isotope ratios and bedrock lithology is not very strong. Studies have found that most rocks have a long-term ($^{234}U/^{238}U$) value at equilibrium (DePaolo et al., 2006). Previous studies indicated that for clays, carbonates, granites, and young volcanic rocks, etc., their U series decay chains are in long-term equilibrium (Sims et al., 1999, 2002; Tricca et al., 2000). These studies also found that U isotope ratios have no clear relationship with the mineral composition or chemical composition of bedrock, based on representative glacial debris from North America, northern and Western Europe, Oceania and New Zealand (DePaolo et al., 2012). Our XRF and XRD measurements showed that the mineral composition of TP dust is overall similar throughout the sampling locations (Tables S1 and S2, Figure S2 in

Supporting Information S1). In particular, our XRD measurements showed that quartz, chlorite, calcite and biotite are the major minerals in the dust samples from all Tibetan sites. Only very small differences were observed in the compositions associated with different locations, thus implying the consistency of geological units and the consistency of mineral and elemental composition of the TP surface dust. The TP surface dust, with similar geological origin, may have experienced similar weathering and sorting processes in different regions during the plateau uplift in historical period.

(c) **Erosion rate**. The erosion rate of the Tibetan Plateau and its surrounding areas is high (ranging from 0.01 to 0.1 mm yr^{-1}, Herman et al., 2013). Based on offshore sedimentary records and the paleotopographic reconstruction from Pliocene to Pleistocene time, it has been thought that river erosion turned to glacier erosion during this period. For example, the tectonically active Himalayan mountains have a much higher erosion rate (in the range of 2–7 mm yr^{-1}), and the orogenic belt can provide large amounts of comminution sediments. These orogenic belts tend to have a landscape dominated by glacial erosion and mass wasting with high rates of erosion. Higher erosion rates are also observed in some tectonically static orogenic belts, but only occurred in areas severely eroded by glaciers, indicating the important role of glacial erosion on erosion overall and the fragmentation of rock particles. Moreover, the erosion rate is low in most other flat areas on the plateau surface.

The intense processes of thermal expansion and contraction, radiation and freeze-thaw dynamics in glacial areas lead to strong physical and chemical weathering and high erosion rates (Dadson et al., 2003; Herman et al., 2013; Larsen et al., 2014). Thus, glacial erosion and rugged topography may provide plenty of freshly comminuted material with short transport times (Lee et al., 2010; Y. K. Li et al., 2014; Ouimet et al., 2009). Conversely, erosion rates become increasingly lower with decreasing altitude. On the flat terrain of the inner plateau surface, the supply of fresh comminution particles is reduced, while surface transport times and residence times are longer – thus resulting in lower ($^{234}U/^{238}U$) values. Therefore, Figure 4 reflects the overall change trend of U isotope comminution age with elevation change. The ($^{234}U/^{238}U$) activity ratios of the comminuted dust particles located near the glaciated areas with rugged topography and increased elevation are closer to the equilibrium value (higher value, see Figures 4 and 5). Tectonic activities and landscape dynamics may cause mass wasting, thereby further enhancing the production of comminution material.

(d) **Geomorphology**. Natural (landform) hazards such as landslides may also have influence on the ($^{234}U/^{238}U$) isotopes distribution of the TP surface dust, as the associated rock fragmentation processes during mass movements. Studies have shown that many large landslides and deep gravity-driven slope deformations occur along major rivers in rapidly uplifting areas, highly undulating hillsides, and narrow river valleys (Agliardi et al., 2013; Ambrosi & Crosta, 2006; Korup et al., 2010; Zhao et al., 2019). According to previous research in the Sanjiangyuan region of the TP, the main natural (landform) hazards include landslide, ground collapse, land freeze-thaw, rockfall and ground subsidence. The main disaster type is landslide, followed by rockfall and ground collapse. In this study, the geomorphic environment of the sampling sites has been mainly the flat area on the plateau (see Figure 2). However, several samples collected from the glacier areas indicated that the TP glaciers constitute zones characterized by strong erosion and fragmentation processes. These latter samples could reflect the intense erosion and particle fragmentation process in the glacier area and rugged terrain. The tectonic activities and landscape dynamics are closely related to the weathering and fragmentation of rock particles, which fundamentally result in certain spatial variation of U isotopes in the sampling areas of various terranes of the TP. The marked differences in topographic relief configurations will cause landslides, multi-step transport processes, thus exerting further influence of eroded material residence time besides the surface evolution processes on ($^{234}U/^{238}U$) values.

Moreover, the scatter relationship between the ($^{234}U/^{238}U$) values and the distance of dust samples to the glacier area are also consistent with the results of the changes in the dust composition with elevation. As shown in Figure 4, dust samples generally show higher ($^{234}U/^{238}U$) ratio with increasing altitude. This observation reflects the higher value of ($^{234}U/^{238}U$) of dust samples in higher altitude areas with faster physical-chemical denudation rates and shorter transport time (L. Li et al., 2017). Although the degree of fit between elevation and ($^{234}U/^{238}U$) values is scattered, we can see from the figure that there is a relatively good positive correlation between ($^{234}U/^{238}U$) values and elevation ($R^2 = 0.64$, $p < 0.01$). This may reflect the combined overall effects of the local sampling landscape dynamic difference and glacial erosion in the sampling areas, such as the geomorphic type of the similar high altitudes (e.g., glacier or non-glacier area, the sampling area slope), the mixture of the comminuted particles from various sources, the distance to glaciers, and the scale of the glaciated erosion zone.

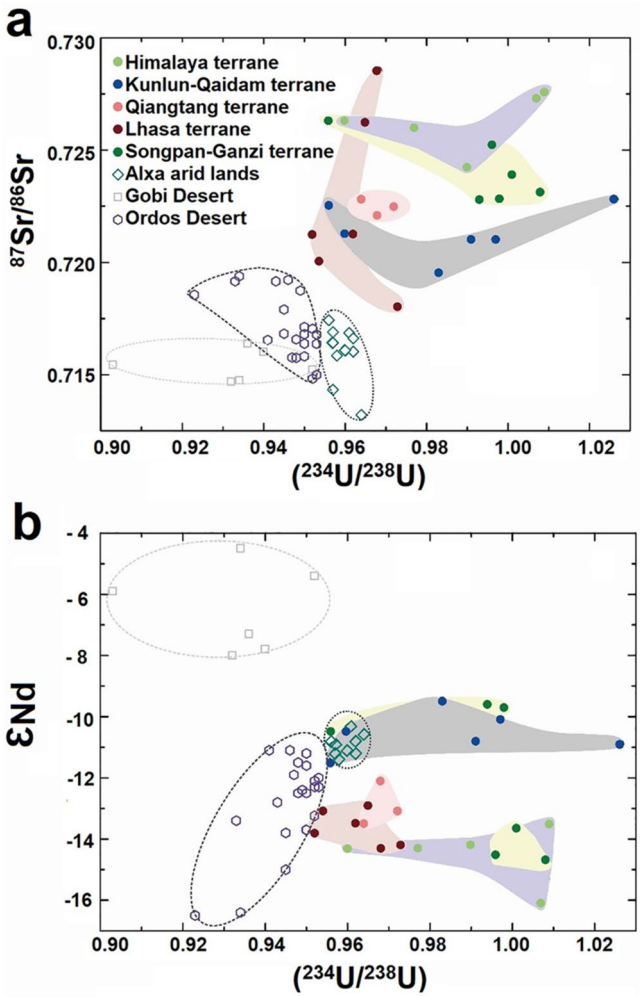

Figure 6. Comparison of the U-Sr-Nd isotopic composition of the Tibetan Plateau with surrounding arid deserts, to indicate the regional difference of TP dust with other dust sources, including the Gobi Desert (south), Alxa arid lands and Ordos Desert (Biscaye et al., 1997; Li et al., 2018; Nakano et al., 2004; Wei et al., 2021).

Here the relationship between TP dust grain size and U isotope scatter with elevation change should be clarified. Usually fine particles move out of equilibrium faster than larger particles. However, this principle varies appreciably only within a certain grain size range. In this study, samples with particle size range of 10–50 μm were selected for U comminution analysis. Within such particle size range, the U isotope comminution age fits within the ideal range, reflecting the overall trend of ($^{234}U/^{238}U$) values decreasing with the increase of age (DePaolo et al., 2006, 2012). Moreover, we find that the particle size composition of the TP dust does not vary much over the various locations considered in our study (Figure S1 in Supporting Information S1). Therefore, the influence of particle size on U isotope should be negligible within the error range, and will not cause much scatter of the U isotope data in the results.

4.2. Comparing U Isotopic Composition of Tibetan Plateau Dust With Surrounding Aeolian Sources and Sinks in the Northern Hemisphere

U-Nd-Sr isotopic composition data were also used to shown the regional differences in this work (Figures 6 and 7). We note that the grain size is an important parameter for Sr isotope analysis. Furthermore, grain size distribution in this study displayed a clear major composition of particles with both clay-sized (<5 μm) and normal Asian dust (<100 μm, with median diameter of 10–20 μm) sections (see Figure S1 in Supporting Information S1), with a good log-normal volume-size distribution; large particles with size >75 μm are rare in the samples, since we collected the arid dust on the plateau surface. This is also relevant for aeolian source emission research in TP, because these size fractions are consistent with atmospherically transported material. The U-Nd-Sr isotopic composition of TP dust is significantly different and unique when compared with that of the major dust source areas in the Asian region (including the East and Central Asian deserts, e.g., the Gobi Desert and Alxa Arid Lands and Ordos Desert; Figures 6a and 6b). The U and Sr isotopic composition of TP dust is generally high, while the εNd is generally low. In addition, the $^{87}Sr/^{86}Sr$ value in the Alxa Arid Lands is relatively low (0.71433–0.71689), and the εNd (−11.4 to −10.3) overlapped the values in north TP (−11.5 to −9.5), while the ($^{234}U/^{238}U$; 0.956–0.964) is lower than that in the north TP (0.956–1.026). The $^{87}Sr/^{86}Sr$ (0.71433–0.71689) and εNd values (−11.4 to −10.3) in the Alxa Arid Lands are similar to those in the Ordos Desert ($^{87}Sr/^{86}Sr$ is 0.71482–0.71939, εNd is −16.5 to −11.1 ($^{234}U/^{238}U$) is 0.956–0.964), but the ($^{234}U/^{238}U$) values in the Alxa Arid Lands are higher than in the Ordos Desert (0.923–0.953). We find that the lowest $^{87}Sr/^{86}Sr$ (the average is 0.91541) and highest εNd (the average is −6.4), and the lowest ($^{234}U/^{238}U$) value (the average is 0.933) in the Gobi Desert are significantly different from the corresponding values in TP dust, Alxa Arid Lands and Ordos Desert (Biscaye et al., 1997; Li et al., 2018; Nakano et al., 2004).

Dust records from snow and ice can preserve both contemporary and paleoclimate-environment information, while high-elevation dust production is sensitive to changes in the atmospheric circulation. Therefore, glacier snowpack dust and cryoconite in the TP have a unique advantage in that they provide information on high-altitude dust processes (Dong et al., 2016, 2020). Studies have shown that arid deserts of the TP are the main source of snowpack/cryoconite dust for glaciers in this region (Dong et al., 2016, 2018). The $^{234}U/^{238}U$ isotopic ratios of typical glacial snowpack/cryoconite samples (including snowpack/cryoconite of the Laohugou Glacier and the Dunkemadi Glacier in this work) combined with the U-Sr-Nd isotope data were used to investigate the contribution of TP dust to the glaciers in surrounding areas. Isotopic compositions of loess in the Loess Plateau and Greenland ice core dust were also used (Li et al., 2018; Lupker et al., 2010) to determine the contribution of TP dust sources to Asian dust sinks and other remote Northern Hemisphere locations.

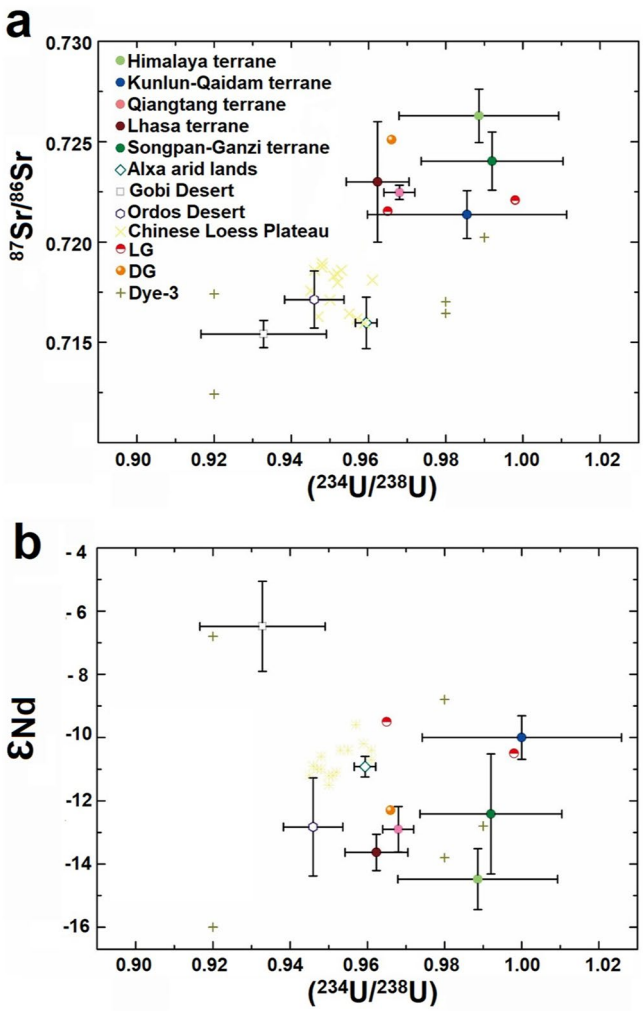

Figure 7. The U-Sr-Nd isotopes of the Tibetan Plateau dust and its comparison with several dust sinks to reflect large-scale dust depositions and cycles, including snowpack/cryoconite dust of glaciers (LG and DG), loess on the Loess Plateau and Greenland ice core dust, which indicated the median and arithmetical distribution of each source and was used to compare the relative contribution to each sink. The center point is the average value, with error bars showing standard error of the mean. Related major dust sources in the Northern Hemisphere, including Gobi Desert (south), Alxa arid lands, Ordos Desert, are also presented in the figure (Biscaye et al., 1997; Li et al., 2018; Lupker et al., 2010; Nakano et al., 2004; Wei et al., 2021).

Figure 7a shows that the U-Sr isotopic compositions of Dunkemadi Glacier were similar to the southern TP dust, but that of Laohugou Glacier was similar to the northern TP dust. The U-Sr isotopic composition of fresh loess on the Loess Plateau overlapped with that of the west TP, Alxa Arid Lands, and Ordos deserts dust, which may constitute areas that contributed aeolian dust to the Loess Plateau. The composition of ($^{234}U/^{238}U$) and $^{87}Sr/^{86}Sr$ in the Greenland ice core dust is more broadly distributed (Figure 7b), which clearly indicates that the dust deposits are similar to dust from north TP and the Gobi Desert. U-Nd isotopic composition of the DG snowpack was similar to western TP dust, and the Laohugou Glacier showed similar U-Nd isotopic composition to the northern TP when compared with U-Sr isotopes. Most loess samples from the Chinese Loess Plateau showed very similar U-Nd isotopes to those of the north TP dust and Alxa Arid Lands. Similarly, the U-Nd isotopic compositions of Greenland ice core dust were also dispersed and somewhat similar to dust from the TP and Gobi Desert.

4.3. Implication for Tracing Aeolian Dust Provenance From U Isotopes Over Large Scales

From the U-Nd-Sr isotopic composition data (Figure 6), we can infer that the dust deposited in the Dunkemadi Glacier area of the central TP is mainly derived from source areas to the western and southern TP. By contrast, the snowpack/cryoconite dust in Laohugou Glacier of the Qilian Mountains mainly originates from northern TP dust (Dong et al., 2014, 2016, 2020; Wei et al., 2017). The dust on the Loess Plateau is mainly affected by dust inputs from north TP, Ordos Desert (Li et al., 2018), Alxa Arid Lands, as well as possible inputs from long-range transported dust from west TP dust and the southern Gobi Desert. Moreover, some Greenland ice core samples showed similar U-Sr-Nd isotopic composition (Lupker et al., 2010) compared with those in the southern Gobi Desert, TP dust and other arid deserts in northwest China (Chen et al., 2007; Dong et al., 2016, 2018; Wei et al., 2019), indicating the potential TP dust transport and inputs to Greenland.

Figure 7 shows the U-Sr-Nd isotopes of the TP soil and its comparison with several dust sinks to reflect large-scale dust deposition patterns, also included are the snowpack/cryoconite dust samples from TP glaciers (Laohugou and Dunkemadi Glaciers), loess on the Loess Plateau, and Greenland ice core dust (Li et al., 2018; Lupker et al., 2010). Based on these observations, we evaluated the relative contribution of different dust sources to dust sinks by using an End-Member Mixing Analysis model (Figure 8) and a constrained least squares approach to derive dust proportions within each sediment or dust sample. This method is adapted from stream chemistry source separation techniques as well as sediment source separation techniques (Brahney et al., 2008). If the dust samples are bound by all potential end-members, the percent contribution of each end-member to the dust can be calculated. The relative contribution of major Northern Hemisphere dust sources to dust sinks were computed and compared with each other by using a εNd–($^{234}U/^{238}U$) mixing space and constrained least squares equations.

Therefore, the potential dust sources include the Gobi Deserts, Alxa Arid Lands, Ordos Desert and TP dust. The error range was determined using Monte Carlo simulations based on the mean and standard deviation of sources. Therefore, the above results show that the Tibetan Plateau may be a significant contributor to dust production and transmission in the Northern Hemisphere. Moreover, several dust sinks (such as the high-altitude TP glacier cryoconites, loess on the Loess Plateau, and Greenland ice core dust) showed similar U-Sr-Nd isotopic compositions to those of the TP dust, implying that the TP dust undergoes long-range transport through large-scale atmospheric

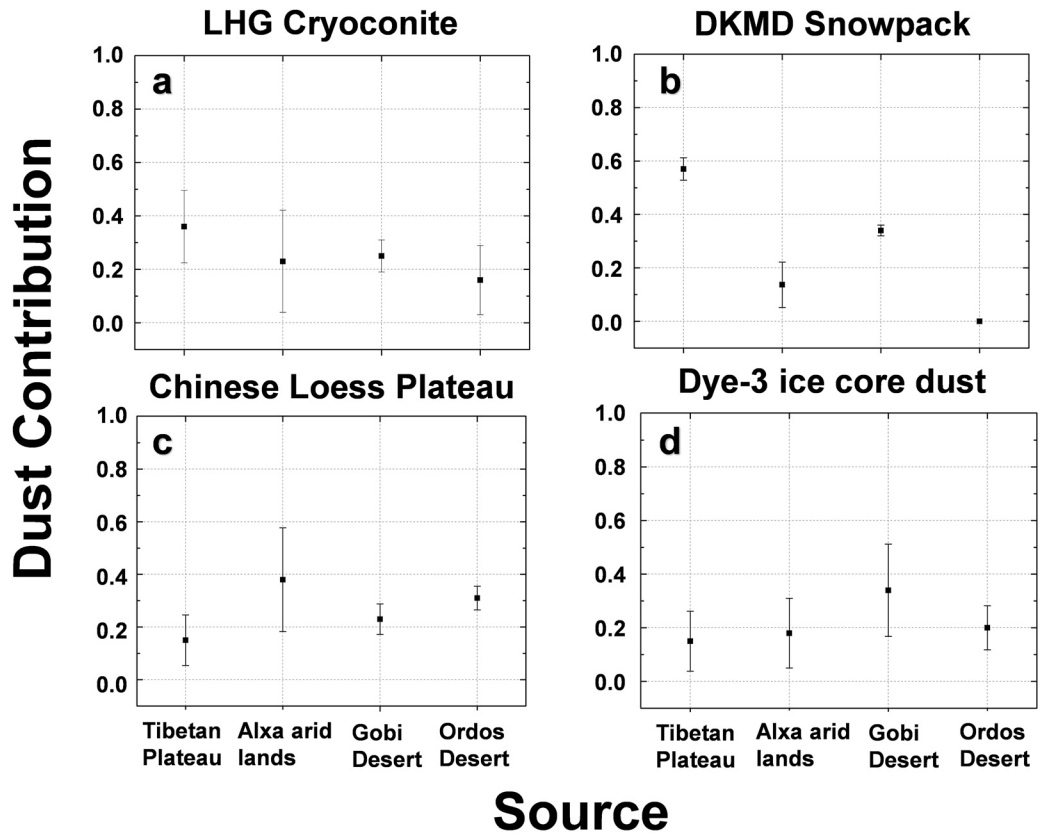

Figure 8. The derived from isotope mixing space model for dust sources and sinks. Tibetan Plateau and the main dust sources in the Northern Hemisphere, including Gobi Desert (south), Alxa arid lands, Ordos Desert, and dust sinks, including snowpack/cryoconite dust of glaciers (Laohugou No.12 Glacier and Dunkemadi Glacier), loess on the Chinese Loess Plateau and Greenland ice core dust (Biscaye et al., 1997; Li et al., 2018; Lupker et al., 2010; Nakano et al., 2004; Wei et al., 2021). The method uses principal components analyses to assign end-member contributions. If the sinks-sediment intervals are bound by all potential end-members, the percent contribution of each end-member to the sediments can be calculated using a constrained least squares equation. Because each end-member is based on several observations, we compute a mean and standard deviation of each end-member (Brahney et al., 2008).

circulation. Therefore, this new constraint on the production and transportation of TP dust provides a new proxy and perspective for aeolian dust evolution and cycling in the TP region.

Besides tracing isotopes (e.g., U, Sr), new methods of meteorology and remote sensing data have also been used to trace dust provenance (Fang et al., 2004). The occurrence of dust storms over the TP and desert of northern China is obvious and atmospheric circulation can influence dust deposition in downwind areas, such as the Chinese Loess Plateau or even the Atlantic Ocean. Previous studies using ground-instrumental and satellite observations have also revealed that the dust raised from northern China can be transported over long distances moving eastward and passing by the Chinese Loess Plateau and North China Plain (Tan et al., 2012). In view of the frequent dust storm occurrence over the TP, and under consideration of the spatial variation in the annual mean number of local dust storm occurrences, we conclude that the TP dust may have significant contribution to aeolian deposition in the surrounding sinks and even in the Greenland ice sheet (Dong et al., 2020; Wei et al., 2021).

Therefore, from the above discussion we find that the ($^{234}U/^{238}U$) isotope provides a proxy for the combined influence of short comminution times (tectonics, landscape dynamic, and glacial erosion) and long residence time on the TP. When compared with other central Asian dust sources, U-Nd-Sr isotope signatures in TP dust are distinct and can be thus used as an effective tracer of dust provenance. This work also demonstrates that TP dust undergoes long-range transport and is probably a potential significant component of the Asian and Northern Hemisphere atmospheric dust aerosol budget.

5. Conclusions

The U comminution age method can be used to trace intermediate phases in the movement of dust from production, through surface transport, to deposition. As such, this method can provide new information on the age of the source materials, the time in transit, as well as the stability of the sink areas. In addition, U isotope characterization from surface soils provides data for a new isotopic tracer of deposited dust. Using this method, we have found that U isotopes in TP's dust are influenced by the combined effect of tectonic activity, high-altitude glacier processes and mass wasting from landscape dynamics (for example, in the form of landslides). The characteristics of U isotopes in the particulate material provide, thus, information that can be useful to better understand the various stages of the Tibetan Plateau's evolution influenced by different environmental and geological processes. The spatial variation showed that the ($^{234}U/^{238}U$) isotope ratios of TP dust was relatively high in the Songpan-Ganzi-Hoh Xil, Himalayan and the Kunlun-Qaidam terranes, and relatively low ($^{234}U/^{238}U$) in Lhasa and Qiangtang terranes. However, among all samples, the highest values occurred in the glaciation zone (e.g., northern TP). Dust collected from nearby glacial areas with rugged terrain (e.g., the Qilian and Himalayan Mountains) displayed higher ($^{234}U/^{238}U$) values than dust collected in the topologically flat non-glacial areas due to their relatively young age.

When comparing the ($^{234}U/^{238}U$) values between different types of sediments at the global scale, the ($^{234}U/^{238}U$) values of TP dust fall between that of river sediments (short transport and deposition time) and dust sink areas (long transport and deposition time). This comparison further indicates that the spatial variation of the ($^{234}U/^{238}U$) values in TP surface dust may be caused by mixing freshly eroded particles with those dust particles of long comminution ages. Given the TP region's unique isotopic composition compared to other major dust-producing regions, the results suggest that TP dust undergoes long-range transport and constitutes a significant fraction of atmospheric dust in the Northern Hemisphere. Dust sink areas with isotopic compositions that reflect TP dust include the high-altitude glaciers (e.g., Laohugou Glacier and Dunkemadi Glacier), Chinese Loess deposits, and the Greenland ice.

An end-member mixing model was used to determine the relative contributions of TP dust to these locations. Together, these isotopic datasets emphasize the strong entrainment potential of TP dusts throughout the Northern Hemisphere. The U isotope comminution method provides a new method to constrain and assess processes of production, evolution, and transport of TP dusts in Asia's high altitude region and in the Northern Hemisphere.

Data Availability Statement

Data of uranium isotopes and X-ray diffraction-X-ray fluorescence spectroscopic analysis measurements in this work has been presented in the tables, figures in the text, and the data analysed in this paper are also available from the Figshare (https://doi.org/10.6084/m9.figshare.19158455).

Conflict of Interest

The authors declare no conflicts of interest relevant to this study.

Acknowledgments
This work was funded by the National Natural Science Foundation of China (42022002), and the State Key Laboratory of Cryosphere Sciences (SKLCS-ZZ-2021). EJRP is funded by the German Research Foundation through the Heisenberg Programme "Multiscale Simulation of Earth Surface Processes", while JB is funded through NSF Critical Zone Collaborative proposal #2011910. The authors would like to thank the field-work team (Chen S., Di J., and Li G.) who worked in the harsh and cold environment on the Tibetan Plateau region during 2017–2020. We also appreciate Prof. Amy East (Editor) and two anonymous reviewers for their helpful comments and suggestions that largely improved the quality of the paper.

References

Aciego, S. M., Bourdon, B., Lupker, M., & Rickli, J. (2009). A new procedure for separating and measuring radiogenic isotopes (U, Th, Pa, Ra, Sr, Nd, Hf) in ice cores. *Chemical Geology*, *266*, 203–213. https://doi.org/10.1016/j.chemgeo.2009.06.003

Agliardi, F., Crosta, G. B., Frattini, P., & Malusa, M. G. (2013). Giant non-catastrophic landslides and the long-term exhumation of the European Alps. *Earth and Planetary Science Letters*, *365*, 263–274. https://doi.org/10.1016/j.epsl.2013.01.030

Aitchison, J. C., Badengzhu, Davis, A. M., Liu, J. B., Luo, H., Malpas, J. G., et al. (2000). Remnants of a Cretaceous intra-oceanic subduction system within the Yarlung-Zangbo suture (southern Tibet). *Earth and Planetary Science Letters*, *183*(1–2), 231–244. https://doi.org/10.1016/s0012-821x(00)00287-9

Ambrosi, C., & Crosta, G. B. (2006). Large sacking along major tectonic features in the Central Italian Alps. *Engineering Geology*, *83*(1–3), 183–200. https://doi.org/10.1016/j.enggeo.2005.06.031

Biscaye, P. E., Grousset, F. E., Revel, M., Van der Gaast, S., Zielinski, G. A., Vaars, A., & Kukla, G. (1997). Asian provenance of glacial dust (stage 2) in the Greenland ice sheet project 2 ice core, summit, Greenland. *Journal of Geophysical Research: Oceans*, *102*, 26765–26781. https://doi.org/10.1029/97jc01249

Bory, A. J. M., Biscaye, P. E., & Grousset, F. E. (2003). Two distinct seasonal Asian source regions for mineral dust deposited in Greenland (North GRIP). *Geophysical Research Letters*, *30*(4), 1167. https://doi.org/10.1029/2002gl016446

Bourdon, B., Bureau, S., Andersen, M. B., Pili, E., & Hubert, A. (2009). Weathering rates from top to bottom in a carbonate environment. *Chemical Geology*, *258*(3–4), 275–287. https://doi.org/10.1016/j.chemgeo.2008.10.026

Bourdon, B., Turner, S., Henderson, G. M., & Lundstrom, C. C. (2003). Introduction to U-series geochemistry. *Reviews in Mineralogy and Geochemistry*, *52*(1), 1–21. https://doi.org/10.1515/9781501509308-006

Brahney, J., Clague, J. J., Menounos, B., & Edwards, T. W. D. (2008). Geochemical reconstruction of late holocene drainage and mixing in kluane lake, yukon territory. *Journal of Paleolimnology*, *40*, 489–505. https://doi.org/10.1007/s10933-007-9177-z

Chabaux, F., Blaes, E., Granet, M., Roupert, R. D., & Stille, P. (2012). Determination of transfer time for sediments in alluvial plains using ^{238}U-^{234}U-^{230}Th disequilibria: The case of the Ganges River system. *Comptes Rendus Geoscience*, *344*(11–12), 688–703. https://doi.org/10.1016/j.crte.2012.10.013

Chen, J., Li, G. J., Yang, J. D., Rao, W. B., Lu, H. Y., Balsam, W., et al. (2007). Nd and Sr isotopic characteristics of Chinese deserts: Implications for the provenances of Asian dust. *Geochimica et Cosmochimica Acta*, *71*(15), 3904–3914. https://doi.org/10.1016/j.gca.2007.04.033

Chen, L., Capitanio, F. A., Liu, L. J., & Gerya, T. (2017). Crustal rheology controls on the Tibetan plateau formation during India-Asia convergence. *Nature Communications*, *8*, 15992. https://doi.org/10.1038/ncomms15992

Chevalier, M. L., Tapponnier, P., van der Woerd, J., Leloup, P. H., Wang, S., Pan, J., et al. (2020). Late quaternary extension rates across the northern half of the yadong-Gulu Rift: Implication for east-west extension in southern tibet. *Journal of Geophysical Research: Solid Earth*, *125*(7), e2019JB019106. https://doi.org/10.1029/2019jb019106

Chung, S. L., Lo, C. H., Lee, T. Y., Zhang, Y. Q., Xie, Y. W., Li, X. H., et al. (1998). Diachronous uplift of the Tibetan plateau starting 40? Myr ago. *Nature*, *394*, 769–773. https://doi.org/10.1038/29511

Dadson, S. J., Hovius, N., Chen, H., Dade, W. B., Hsieh, M. L., Willett, S. D., et al. (2003). Links between erosion, runoff variability and seismicity in the Taiwan orogen. *Nature*, *426*, 648–651. https://doi.org/10.1038/nature02150

Decelles, P. G., Gehrels, G. E., Quade, J., Lareau, B., & Spurlin, M. (2000). Tectonic implications of U-Pb Zircon ages of the himalayan orogenic belt in Nepal. *Science*, *288*(5465), 497–499. https://doi.org/10.1126/science.288.5465.497

Deng, B., Liu, S. G., Enkelmann, E., Li, Z. W., Ehlers, T. A., & Jansa, L. (2015). Late Miocene accelerated exhumation of the Daliang Mountains, Southeastern margin of the Tibetan plateau. *International Journal of Earth Science*, *104*(4), 1061–1081. https://doi.org/10.1007/s00531-014-1129-z

DePaolo, D. J., Lee, V. E., Christensen, J. N., & Maher, K. (2012). Uranium comminution ages: Sediment transport and deposition time scales. *Comptes Rendus Geoscience*, *344*(11–12), 678–687. https://doi.org/10.1016/j.crte.2012.10.014

DePaolo, D. J., Maher, K., Christensen, J. N., & McManus, J. (2006). Sediment transport time measured with U-series isotopes: Results from ODP North Atlantic drift site 984. *Earth and Planetary Science Letters*, *248*(1–2), 394–410. https://doi.org/10.1016/j.epsl.2006.06.004

Dong, Z. B., Hu, G. Y., Qian, G. Q., Lu, J. F., Zhang, Z. C., Luo, W. Y., et al. (2017). High-altitude aeolian research on the Tibetan plateau. *Reviews of Geophysics*, *55*, 864–901. https://doi.org/10.1002/2017RG000585

Dong, Z. W., Brahney, J., Kang, S. C., Elser, J., Wei, T., Jiao, X. Y., et al. (2020). Aeolian dust transport, cycle and influences in high-elevation cryosphere of the Tibetan Plateau region: New evidences from alpine snow and ice. *Earth-Science Reviews*, *211*, 103408. https://doi.org/10.1016/j.earscirev.2020.103408

Dong, Z. W., Kang, S. C., Qin, D. H., Li, Y., Wang, X. J., Ren, J. W., et al. (2016). Provenance of cryoconite deposited on the glaciers of the Tibetan Plateau: New insights from Nd-Sr isotopic composition and size distribution. *Journal of Geophysical Research: Atmospheres*, *121*(12), 7371–7382. https://doi.org/10.1002/2016jd024944

Dong, Z. W., Qin, D. H., Chen, J. Z., Qin, X., Ren, J. W., Cui, X. Q., et al. (2014). Physicochemical impacts of dust particles on alpine glacier meltwater at the Laohugou Glacier basin in western Qilian Mountains, China. *The Science of the Total Environment*, *493*, 930–942. https://doi.org/10.1016/j.scitotenv.2014.06.025

Dong, Z. W., Shao, Y. P., Qin, D. H., Kang, S. C., Wei, T., Wang, X., et al. (2018). Hf-Nd-Sr isotopic composition as fingerprint for long-range transported eolian dust deposition in glacier snowpack of eastern Tibetan Plateau. *Journal of Geophysical Research: Atmospheres*, *123*(13), 7013–7023. https://doi.org/10.1029/2018jd028581

Dosseto, A., Bourdon, B., Gailardet, J., Allegre, C. J., & Filizola, N. (2006). Time scale and conditions of weathering under tropical climate: Study of the Amazon basin with U-series. *Geochimica et Cosmochimica Acta*, *70*(1), 71–89. https://doi.org/10.1016/j.gca.2005.06.033

Dosseto, A., Turner, S. P., & Douglas, G. B. (2006). Uranium-series isotopes in colloids and suspended sediments: Timescale for sediment production and transport in the Murray–Darling River system. *Earth and Planetary Science Letters*, *246*(3–4), 418–431. https://doi.org/10.1016/j.epsl.2006.04.019

Dou, Y. G., Yang, S. Y., Shi, X. F., Clift, P. D., Liu, S. F., Liu, J. H., et al. (2016). Provenance weathering and erosion records in southern Okinawa Trough sediments since 28 ka: Geochemical and Sr–Nd–Pb isotopic evidences. *Chemical Geology*, *425*, 93–109. https://doi.org/10.1016/j.chemgeo.2016.01.029

Fang, X. M., Han, Y. X., Ma, J. M., Song, L. C., Yang, S. L., & Zhang, X. Y. (2004). Dust storms and loess accumulation on the Tibetan plateau: A case study of dust event on 4 March 2003 in Lhasa. *Chinese Science Bulletin*, *49*(9), 953–960. https://doi.org/10.1007/bf03184018

Francke, A., Dosseto, A., Just, J., Wagner, B., & Jones, B. G. (2020). Assessment of the controls on (^{234}U/^{238}U) activity ratios recorded in detrital lacustrine sediments. *Chemical Geology*, *550*, 119698. https://doi.org/10.1016/j.chemgeo.2020.119698

Gan, W. J., Zhang, P. Z., Shen, Z. K., Niu, Z. J., Wang, M., Wang, Y. G., et al. (2007). Present-day crustal motion within the Tibetan Plateau inferred from GPS measurements. *Journal of Geophysical Research: Solid Earth*, *112*(B8), 416–430. https://doi.org/10.1029/2005jb004120

Granet, M., Chabaux, F., Stille, P., Lanord, C. F., & Pelt, E. (2007). Time-scales of sedimentary transfer and weathering processes from U-series nuclides: Clues from the Himalayan Rivers. *Earth and Planetary Science Letters*, *261*(3–4), 389–406. https://doi.org/10.1016/j.epsl.2007.07.012

Haider, V. L., Dunkl, I., Eynatten, H. V., Ding, L., Frei, D., & Zhang, L. Y. (2013). Cretaceous to Cenozoic evolution of the northern Lhasa terrane and the early paleogene development of peneplains at Nam Co, Tibetan plateau. *Journal of Asian Earth Sciences*, *70–71*, 79–98. https://doi.org/10.1016/j.jseaes.2013.03.005

Han, Y., Fang, X., Zhao, T., Bai, H., Kang, S., & Song, L. (2009). Suppression of precipitation by dust particles originated in the Tibetan Plateau. *Atmospheric Environment*, *43*(3), 568–574. https://doi.org/10.1016/j.atmosenv.2008.10.018

Handley, H., Turner, S., Afonso, J., Dosseto, A., & Cohen, T. (2013). Sediment residence times constrained by uranium-series isotopes: A critical appraisal of the comminution approach. *Geochimica et Cosmochimica Acta*, *103*, 245–262. https://doi.org/10.1016/j.gca.2012.10.047

Harrison, T. M., Copeland, P., Kidd, W. S. F., & Yin, A. (1992). Raising Tibet. *Science*, *255*, 1663–1670. https://doi.org/10.1126/science.255.5052.1663

Herman, F., Seward, D., Valla, P. G., Carter, A., Kohn, B., Willett, S. D., et al. (2013). Worldwide acceleration of mountain erosion under a cooling climate. *Nature*, *504*, 423–426. https://doi.org/10.1038/nature12877

Jin, X., Chen, L., Chen, H., Zhang, W., Wang, W., Ji, H., et al. (2021). XRD and TEM analyses of a simulated leached rare earth ore deposit: Implications for clay mineral contents and structural evolution. *Ecotoxicology and Environmental Safety*, *225*, 112728. https://doi.org/10.1016/j.ecoenv.2021.112728

Jin, X. C., Wang, J., Chen, B. W., & Ren, L. D. (2003). Cenozoic depositional sequences in the piedmont of the west Kunlun and their paleogeographic and tectonic implications. *Journal of Asian Earth Science*, *21*(7), 755–765. https://doi.org/10.1016/s1367-9120(02)00073-1

Korup, O., Densmore, A. L., & Schlunegger, F. (2010). The role of landslides in mountain range evolution. *Geomorphology*, *120*(1–2), 77–90. https://doi.org/10.1016/j.geomorph.2009.09.017

Larsen, I. J., Montgomery, D. R., & Greenberg, H. M. (2014). The contribution of mountains to global denudation. *Geology*, *42*(6), 527–530. https://doi.org/10.1130/g35136.1

Lee, V. E., DePaolo, D. J., & Christensen, J. N. (2010). Uranium-series comminution ages of continental sediments: Case study of a Pleistocene alluvial fan. *Earth and Planetary Science Letters*, *296*(3–4), 244–254. https://doi.org/10.1016/j.epsl.2010.05.005

Li, C., Yang, S. Y., Zhao, J. X., Dosseto, A., Bi, L., & Clark, T. R. (2016). The time scale of river sediment source-to-sink processes in East Asia. *Chemical Geology*, *446*, 138–146. https://doi.org/10.1016/j.chemgeo.2016.06.012

Li, G. J., Li, L., Xu, S. J., Li, X. S., & Chen, J. (2017). Dust source of the loess deposits in the eastern China constrained by uranium comminution age. *Quaternary Sciences*, *37*(5), 1034–1044. (In Chinese). https://doi.org/10.11928/j.issn.1001-7410.2017.05.11

Li, H. B., Pan, J. W., Sun, Z. M., Si, J. L., Pei, J. L., Liu, D. L., et al. (2021). Continental tectonic deformation and seismic activity: A case study from the Tibetan plateau. *Acta Geologica Sinica*, *95*(1), 194–213. (In Chinese).

Li, J. J., Zhou, S. Z., Zhao, Z. J., & Zhang, J. (2015). The Qingzang movement: The major uplift of the Qinghai-Tibetan Plateau. *Science China Earth Sciences*, *58*, 2113–2122. (In Chinese). https://doi.org/10.1007/s11430-015-5124-4

Li, L., Chen, J., Chen, Y., Hedding, D. W., Li, T., Li, L. F., et al. (2018). Uranium isotopic constraints on the provenance of dust on the Chinese Loess Plateau. *Geology*, *46*(9), 747–750. https://doi.org/10.1130/g45130.1

Li, L., Liu, X. J., Li, T., Li, L. F., Zhao, L., Ji, J. F., et al. (2017). Uranium comminution age tested by the eolian deposits on the Chinese Loess Plateau. *Earth and Planetary Science Letters*, *467*, 64–71. https://doi.org/10.1016/j.epsl.2017.03.014

Li, Y. (2014). *Clay mineral composition of soil on the grassland and its environmental significance (in Chinese)*. Master Thesis (Vol. 1−43). Sun Yat-sen University.

Li, Y. K., Li, D. W., Liu, G. N., Harbor, J., Caffee, M., & Stroeven, A. P. (2014). Patterns of landscape evolution on the central and northern Tibetan Plateau investigated using in-situ produced ^{10}Be concentrations from river sediments. *Earth and Planetary Science Letters*, *398*, 77–89. https://doi.org/10.1016/j.epsl.2014.04.045

Li, Y. L., Wang, C. S., Dai, J. G., Xu, G. Q., Hou, Y. L., & Li, X. H. (2015). Propagation of the deformation and growth of the Tibetan-himalayan orogen: A review. *Earth-Science Reviews*, *143*, 36–61. https://doi.org/10.1016/j.earscirev.2015.01.001

Liu, C., Zhu, B. J., Yang, X. L., & Shi, Y. L. (2015). Crustal rheology control on earthquake activity across the eastern margin of the Tibetan Plateau: Insights from numerical modelling. *Journal of Asian Earth Sciences*, *100*, 20–30. https://doi.org/10.1016/j.jseaes.2015.01.001

Liu, S. Z., Xu, X. W., Klinger, Y., Nocquet, J. K., Chen, G. H., Yu, G. H., et al. (2019). Lower crustal heterogeneity beneath the northern Tibetan plateau constrained by GPS measurements following the 2001 Mw7.8 kokoxili earthquake. *Journal of Geophysical Research: Solid Earth*, *124*(11), 11992–12022. https://doi.org/10.1029/2019jb017732

Lupker, M., Aciego, S. M., Bourdon, B., Schwander, J., & Stocker, T. F. (2010). Isotopic tracing (Sr, Nd, U and Hf) of continental and marine aerosols in an 18th century section of the Dye-3 ice core (Greenland). *Earth and Planetary Science Letters*, *295*(1–2), 277–286. https://doi.org/10.1016/j.epsl.2010.04.010

Maher, B. A., Prospero, J. M., Mackie, D., Gaiero, D., Hesse, P. P., & Balkanski, Y. (2010). Global connections between aeolian dust, climate and ocean biogeochemistry at the present day and at the last glacial maximum. *Earth-Science Reviews*, *99*(1–2), 61–97. https://doi.org/10.1016/j.earscirev.2009.12.001

Mao, R., Gong, D. Y., Shao, Y. P., Wu, G. J., & Bao, J. D. (2013). Numerical analysis for contribution of the Tibetan Plateau to dust aerosols in the atmosphere over the East Asia. *Science China Earth Sciences*, *56*, 301–310. https://doi.org/10.1007/s11430-012-4460-x

Mao, R., Hu, Z. Y., Zhao, C., Gong, D. Y., Guo, D., & Wu, G. J. (2019). The source contributions to the dust over the Tibetan plateau: A modelling analysis. *Atmospheric Environment*, *214*, 116859. https://doi.org/10.1016/j.atmosenv.2019.116859

Mulch, A., & Chamberlain, C. P. (2006). Earth science: The rise and growth of Tibet. *Nature*, *439*, 670–671. https://doi.org/10.1038/439670a

Nakano, T., Yokoo, Y., Nishikawa, M., & Koyanagi, H. (2004). Regional Sr–Nd isotopic ratio of soil minerals in northern China as Asian dust fingerprints. *Atmospheric Environment*, *38*(19), 3061–3067. https://doi.org/10.1016/j.atmosenv.2004.02.016

Osterberg, E., Mayewski, P., Kreutz, K., Fisher, D., Handley, M., Sneed, S., et al. (2008). Ice core record of rising lead pollution in the North Pacific atmosphere. *Geophysical Research Letters*, *35*(5), L05810. https://doi.org/10.1029/2007gl032680

Ouimet, W., Whipple, K., & Granger, D. E. (2009). Beyond threshold hillslopes Channel adjustment to base-level fall in tectonically active mountain ranges. *Geology*, *37*(7), 579–582. https://doi.org/10.1130/g30013a.1

Ouimet, W., Whipple, K., Royden, L., Reiners, P., Hodges, K., & Pringle, M. (2010). Regional incision of the eastern margin of the Tibetan Plateau. *Lithosphere*, *2*(1), 50–63. https://doi.org/10.1130/l57.1

Owen, L. A., Finkel, R. C., Ma, H. Z., & Barnard, P. L. (2006). Late quaternary landscape evolution in the Kunlun Mountains and Qaidam Basin, northern Tibet: A framework for examining the links between glaciation, lake level changes and alluvial fan formation. *Quaternary International*, *154–155*, 73–86. https://doi.org/10.1016/j.quaint.2006.02.008

Pan, B. T., Gao, H. S., Li, B. Y., & Li, J. J. (2004). Step-like landforms and uplift of the Qinghai-Xizang plateau. *Quaternary Sciences*, *24*(1), 50–57. (In Chinese).

Pan, B. T., Su, H., Hu, Z. B., Hu, X. F., Gao, H. S., Li, J. J., et al. (2009). Evaluating the role of climate and tectonics during steady incision of the yellow river: Evidence from a 1.24 Ma terrace record near Lanzhou, China. *Quaternary Science Reviews*, *28*(27–28), 3281–3290. https://doi.org/10.1016/j.quascirev.2009.09.003

Pettke, T., Lee, D. C., Halliday, A. N., & Rea, D. K. (2002). Radiogenic Hf isotopic compositions of continental eolian dust from Asia, its variability and its implications for seawater Hf. *Earth and Planetary Science Letters*, *202*(2), 453–464. https://doi.org/10.1016/s0012-821x(02)00778-1

Prospero, J. M., Ginoux, P., Torres, O., Nicholson, S. E., & Gill, T. E. (2002). Environmental characterization of global sources of atmospheric soil dust identified with the Nimbus 7 Total Ozone Mapping Spectrometer (TOMS) absorbing aerosol product. *Reviews of Geophysics*, *40*(1), 1002. https://doi.org/10.1029/2000rg000095

Royden, L. H., Burchfiel, B. C., & Van der Hilst, R. D. (2008). The geological evolution of the Tibetan Plateau. *Science*, *321*(5892), 1054–1058. https://doi.org/10.1126/science.1155371

Sims, K., Depaolo, D. J., Murrell, M. T., Baldridge, W. S., Goldstein, S., Clague, D., et al. (1999). Porosity of the melting zone and variations in the solid mantle upwelling rate beneath Hawaii: Inferences from ^{238}U-^{230}Th-^{226}Ra and ^{235}U-^{231}Pa disequilibria. *Geochimica et Cosmochimica Acta*, *63*(23–24), 4119–4138. https://doi.org/10.1016/s0016-7037(99)00313-0

Sims, K., Goldstein, S., Blichert-Toft, J., Perfit, M. R., Kelemen, P., Fornari, D. J., et al. (2002). Chemical and isotopic constraints on the generation and transport of magma beneath the East Pacific Rise. *Geochimica et Cosmochimica Acta*, *66*(19), 3481–3504. https://doi.org/10.1016/s0016-7037(02)00909-2

Stibal, M., Sabacka, M., & Zarsky, J. (2012). Biological processes on glacier and ice sheet surfaces. *Nature Geosciences*, *5*(11), 771–774. https://doi.org/10.1038/ngeo1611

Sun, H., Liu, X. D., & Pan, Z. T. (2017). Direct radiative effects of dust aerosols emitted from the Tibetan Plateau on the East Asian summer monsoon – A regional climate model simulation. *Atmospheric Chemistry and Physics*, *17*(22), 13731–13745. https://doi.org/10.5194/acp-17-13731-2017

Sun, J. M. (2005). Nd and Sr isotopic variations in Chinese eolian deposits during the past 8 Ma: Implications for provenance change. *Earth and Planetary Science Letters*, *240*, 454–466. https://doi.org/10.1016/j.epsl.2005.09.019

Takeuchi, N., & Li, Z. (2008). Characteristics of surface dust on Urumqi glacier No. 1 in the tien Shan mountains, China. *Arctic Antarctic and Alpine Research*, *40*, 744–750. https://doi.org/10.1657/1523-0430(07-094)[takeuchi]2.0.co;2

Tan, S. C., Shi, G. Y., & Wang, H. (2012). Long-range transport of spring dust storms in Inner Mongolia and impact on the China seas. *Atmospheric Environment*, *46*, 299–308. https://doi.org/10.1016/j.atmosenv.2011.09.058

Tapponnier, P., Zhiqin, X., Roger, F., Meyer, B., Arnaud, N., Wittlinger, G., et al. (2001). Oblique stepwise rise and growth of the Tibet Plateau. *Science*, *294*(5547), 1671–1677. https://doi.org/10.1126/science.105978

Tricca, A., Porcelli, D., & Wasserburg, G. J. (2000). Factors controlling the groundwater transport of U, Th, Ra, and Rn. *Journal of Earth System Science*, *109*(1), 95–108. https://doi.org/10.1007/bf02719153

Uno, I., Eguchi, K., Yumimoto, K., Toshihiko, T., Shimizu, A., Uematsu, M., et al. (2009). Asian dust transported one full circuit around the globe. *Nature Geosicence*, *2*, 557–560. https://doi.org/10.1038/ngeo583

Vigier, N., Burton, K. W., Gislason, S. R., Rogers, N. W., Duchene, S., Thomas, L., et al. (2006). The relationship between riverine U-series disequilibria and erosion rates in a basaltic terrain. *Earth and Planetary Science Letters*, *249*(3–4), 258–273. https://doi.org/10.1016/j.epsl.2006.07.001

Wang, Q., Zhang, P. Z., Freymueller, J. T., Bilham, R., Larson, K. M., Lai, X. A., et al. (2001). Present-Day crustal deformation in China constrained by global positioning system measurements. *Science*, *294*(5542), 574–577. https://doi.org/10.1126/science.1063647

Wang, W., Qiao, X. J., Yang, S. M., & Wang, D. J. (2017). Present-day velocity field and block kinematics of Tibetan Plateau from GPS measurements. *Geophysical Journal International*, *208*(2), 1088–1102. https://doi.org/10.1093/gji/ggw445

Wang, X. Y., Lu, H. Y., Vandenberghe, J., Zheng, S. H., & Balen, R. V. (2012). Late Miocene uplift of the NE Tibetan Plateau inferred from basin filling, planation and fluvial terraces in the Huang Shui catchment. *Global and Planetary Change*, *88–89*, 10–19. https://doi.org/10.1016/j.gloplacha.2012.02.009

Wei, T., Brahney, J., Dong, Z. W., Kang, S. C., Zong, C. L., Guo, J. M., et al. (2021). Hf−Nd−Sr isotopic composition of the Tibetan Plateau dust as a fingerprint for regional to hemispherical transport. *Environmental Science & Technology*, *55*(14), 10121–10132. https://doi.org/10.1021/acs.est.0c04929

Wei, T., Dong, Z. W., Kang, S. C., Qin, X., & Guo, Z. L. (2017). Geochemical evidence for sources of surface dust deposited on the Laohugou glacier, Qilian Mountains. *Applied Geochemistry*, *79*, 1–8. https://doi.org/10.1016/j.apgeochem.2017.01.024

Wei, T., Dong, Z. W., Kang, S. C., Rostami, M., Ulbrich, S., & Shao, Y. P. (2019). Hf-Nd-Sr isotopic fingerprinting for aeolian dust deposited on glaciers in the northeastern Tibetan Plateau region. *Global and Planetary Change*, *177*, 69–80. https://doi.org/10.1016/j.gloplacha.2019.03.015

Wu, G. J., Zhang, C. L., Zhang, X. L., Tian, L. D., & Yao, T. D. (2010). Sr and Nd isotopic composition of dust in Dunde ice core, Northern China: Implications for source tracing and use as an analogue of long-range transported Asian dust. *Earth and Planetary Science Letters*, *299*(3–4), 409–416. https://doi.org/10.1016/j.epsl.2010.09.021

Wu, Y. Q., Cui, Z. J., Liu, G. N., Ge, D. K., Yin, J. R., Xu, Q. H., et al. (2001). Quaternary geomorphological evolution of the Kunlun pass area and uplift of the Qinghai-Xizang (Tibet) plateau. *Geomorphology*, *36*(3–4), 203–216. https://doi.org/10.1016/s0169-555x(00)00057-x

Xu, Y., Zhang, F., & Jin, Z. D. (2019). Uranium isotopic compositions of fine detrital particles in a glacial catchment of the Pamir Plateau and its implication for sediment transfer. *Journal of Earth Environment*, *10*(2), 116–127. (In Chinese).

Xu, Z. Q., Li, H. B., & Yang, J. S. (2006). An orogenic plateau: The orogenic collage and orogenic types of the Qinghai-Tibet Plateau. *Earth Science Frontiers*, *13*(4), 1–17. (In Chinese).

Yang, X. P., Zhu, B. Q., & White, P. D. (2007). Provenance of aeolian sediment in the Taklimakan Desert of western China, inferred from REE and major-elemental data. *Quaternary International*, *175*(1), 71–85. https://doi.org/10.1016/j.quaint.2007.03.005

Yin, A. (2006). Cenozoic tectonic evolution of the Himalayan orogen as constrained by a long-strike variation of structural geometry, exhumation history, and foreland sedimentation. *Earth-Science Reviews*, *76*(1–2), 1–131. https://doi.org/10.1016/j.earscirev.2005.05.004

Zhang, P. Z., Molnar, P., & Xu, X. W. (2007). Late quaternary and present-day rates of slip along the Altyn Tagh Fault, northern margin of the Tibetan Plateau. *Tectonics*, *26*(5), TC5010. https://doi.org/10.1029/2006tc002014

Zhang, X. Y. (2001). Source distributions, emission, transport, deposition of Asian dust and Loess accumulation (in Chinese). *Quaternary Sciences*, *21*(1), 29–40.

Zhang, X. Y., Gong, S. L., Shen, Z. X., Mei, F. M., Xi, X. X., Liu, L. C., et al. (2003). Characterization of soil dust aerosol in China and its transport and distribution during 2001 ACE-Asia: 1. Network observations. *Journal of Geophysical Research*, *108*(D9), 4261. https://doi.org/10.1029/2002jd002632

Zhao, S. Y., Chigira, M., & Wu, X. Y. (2019). Gigantic rockslides induced by fluvial incision in the Diexi area along the eastern margin of the Tibetan Plateau. *Geomorphology*, *338*, 27–42. https://doi.org/10.1016/j.geomorph.2019.04.008

Zheng, D., & Zhao, D. S. (2017). Characteristics of natural environment of the Tibetan Plateau. *Science and Technology Review*, *35*(6), 13–22. (In Chinese).

Zheng, H. B., Huang, X. T., & Butcher, K. (2006). Lithostratigraphy, petrography and facies analysis of the Late Cenozoic sediments in the foreland basin of the West Kunlun. *Palaeogeography, Palaeoclimatology, Palaeoecology*, *241*(1), 61–78. https://doi.org/10.1016/j.palaeo.2006.06.015